SPIN AND B-FIELD EVOLUTION OF NEUTRON STARS (+ BH SPIN)

AEI IMPRS GW LECTURES 3+4

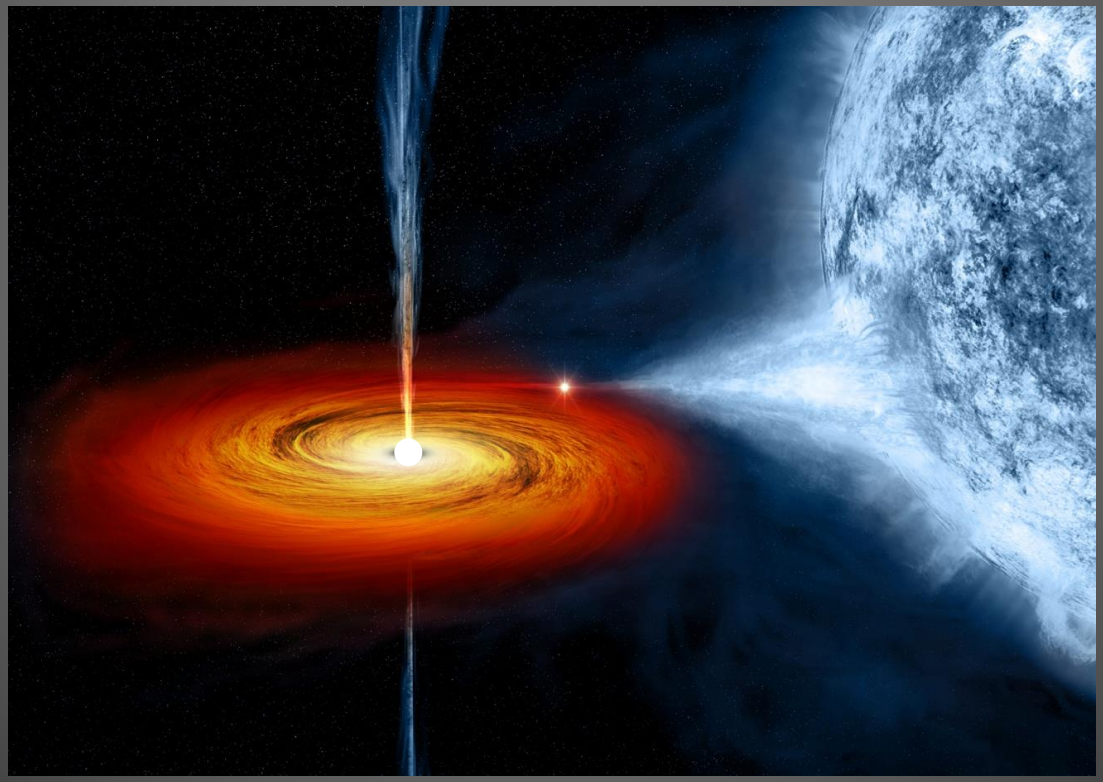

Thomas Tauris – IFA, Aarhus University

Note: These lectures will be recorded and posted onto the IMPRS website

Dear participants,

We will record all lectures on “The Astrophysics of Compact Objects”, including possible Q&A after the presentation, and we will make the recordings publicly available on the IMPRS lecture website at:

https://imprs-gw-lectures.aei.mpg.de

By participating in this Zoom meeting, you are giving your explicit consent to the recording of the lecture and the publication of the recording on the course website.

Albert-Einstein Institute Lectures 2021

Thomas Tauris @ Aarhus University

Lectures 1+2: Wednesday May 12, 10:00 – 12:00

X-ray Binaries and Recycling Millisecond Pulsars

Lectures 3+4: Friday May 14, 10:00 – 12:00

Spin and B-field Evolution of Neutron Stars (+ Black Hole Spins)

Lectures 5+6: Wednesday May 19, 10:00 – 12:00

Formation of Binary Neutron Stars/Black Holes

Lectures 7+8: Friday May 21, 10:00 – 12:00

Binary Neutron Stars and Gravitational Waves at Low and High Frequencies

You are most welcome to ask questions any time ☺

SPIN AND B-FIELD EVOLUTION OF NEUTRON STARS (+ BLACK HOLE SPIN)

AEI LECTURES 3+4

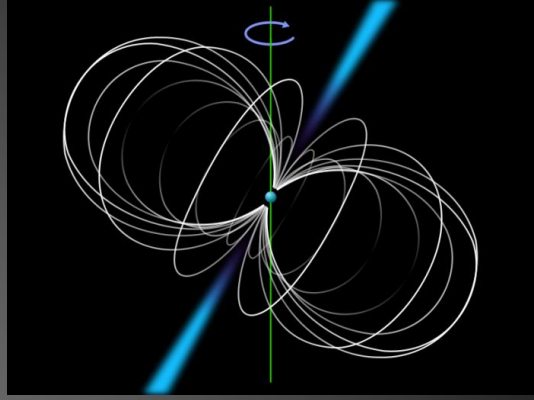

- Observational aspects of radio pulsars
  - The radio pulsar population in the Milky Way
  - Pulse profiles / Scintillation / Dispersion measure
  - Emission properties
- Spin evolution of pulsars in the *PP*-diagram
  - The magnetic dipole model
  - Gravitational wave emission
  - Evolution with B-field decay
  - Evolution with gravitational wave emission
  - The braking index
  - True ages of radio pulsars

Self-study of equations

- Magnetars
  - Soft gamma-ray repeaters (SGRs) and Anomalous X-ray pulsars (AXPs)
- BH spins
  - BHs in X-ray binaries (continuum spectrum fitting)
  - Origin and evolution of X- binary BH spins

Radio Pulsars

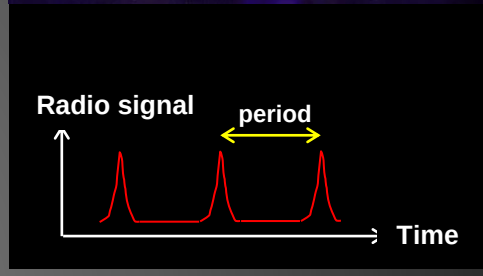

A pulsar is a perfect physics laboratory:

- ✓ ν = 700 Hz (P=1,4 ms – 23 sec.)
- ✓ B = 10^{13} G
- ✓ $\dot{E}_{rot} = 10^{5}\ L_{\odot}$ ($F = 10^{14}\ F_{\odot}$)
- ✓ $M = 1.4\ M_{\odot}$
- ✓ R = 10 km

Giant atomic nucleus:

- ✓ A=10^{57} baryons, ρ_{core} = 2-10 $\rho_{nuclear}$

Magnetosphere:

- ✓ production of 10^{38} (e^-, e^+) per second
- ✓ TeV γ-rays
- ✓ e^- accelerated to 10^{16}eV, $\Delta\phi = 10^{16}$ Volts

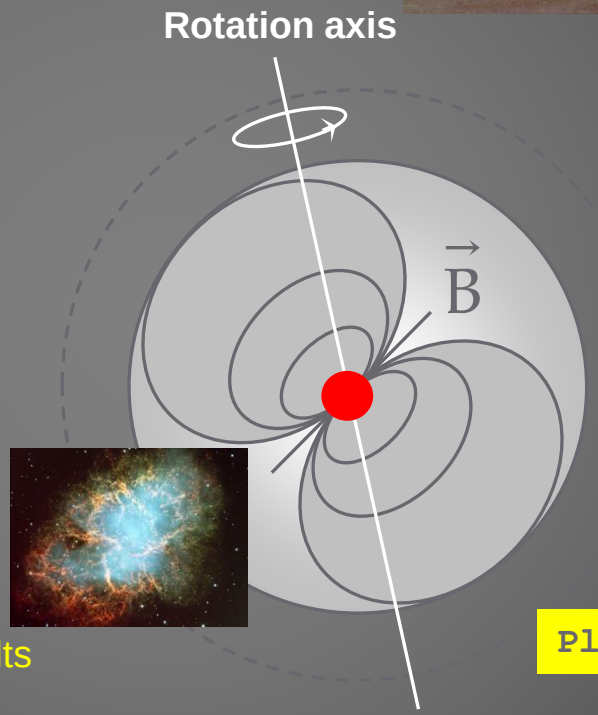

Perfect clock:

- ✓ P = 0.001 557 806 448 872 75 seconds (PSR 1937+21)

Particle physics

Nuclear physics

Solid state physics

Atom physics

Plasma physics

Relativity

Radio Pulsar Emission

The surface intensity of the radio emission, I using a Planck function demonstrates that if the radio emission was caused by thermal black body radiation one would obtain an extremely high brightness temperature (leading to absurdly large particle energies) and therefore the radiation mechanism of a radio pulsar *must* be coherent (Most models invoke curvature radiation or a maser mechanism).

$$I_\nu = \frac{2h\nu^3}{c^2}\frac{1}{e^{h\nu/kT}-1} \qquad \left(I_\nu \propto \nu^{\alpha},\ \alpha = -1.5\right)$$

Planck function — Empirical evidence

$$Crab: \quad f = 0.48\ Jy \quad @\ 436\ MHz$$

$$(1\ Jansky = 10^{-23}\ erg\ cm^{-2}\ s^{-1}\ Hz^{-1}\ st^{-1})$$

Spectral flux density

$$\Rightarrow \quad kT \approx 10^{24}\ eV \quad (T \approx 10^{29}\ K)$$

$$\tilde{S}_{400} = 10\ mJy$$

$$1\ Jy \equiv 10^{-26}\ \frac{W}{m^2 \cdot Hz}$$

Effelsberg 100 m

Sardinia 64 m

Parkes 64 m

$$\sum E^{radio}_{pulsar} \ll E^{kin}_{\mathrm{corn},\,1m}$$

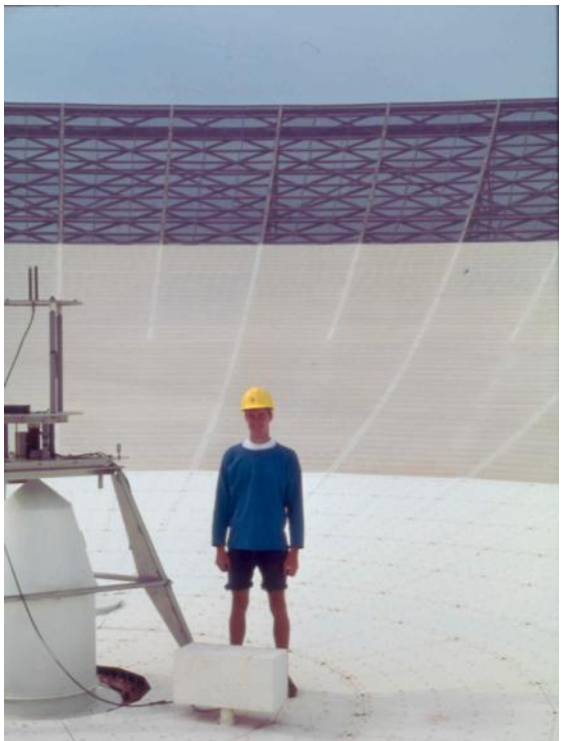

Detected radio pulsars in our Milky Way:

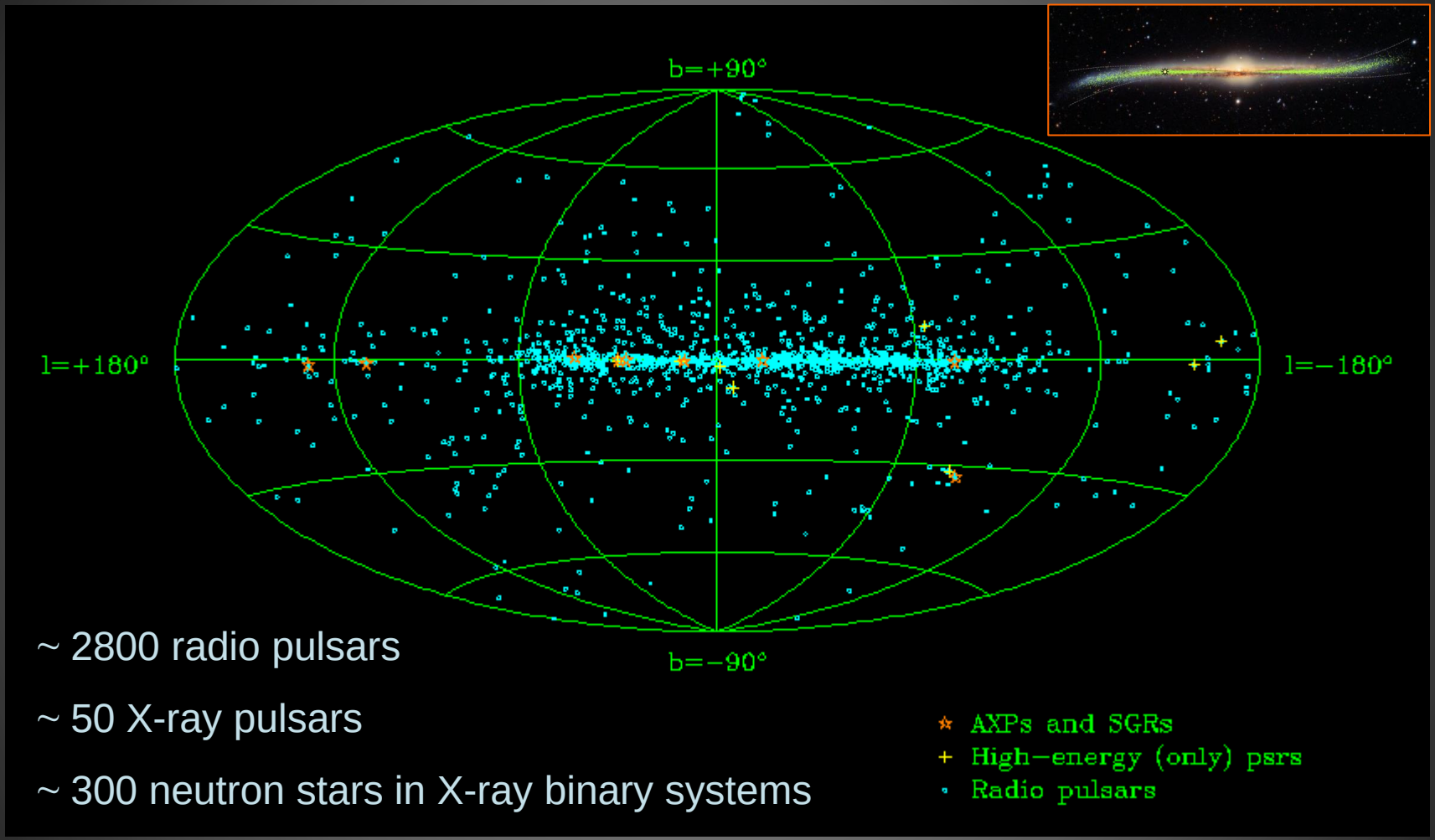

~ 2800 radio pulsars

~ 50 X-ray pulsars

~ 300 neutron stars in X-ray binary systems

- Pulsars are concentrated in the Galactic plane in star forming regions (OB star progenitors)
- Large spread is caused by high velocities (kicks imparted to NSs in supernova explosions)

Detected radio pulsars in our Milky Way:

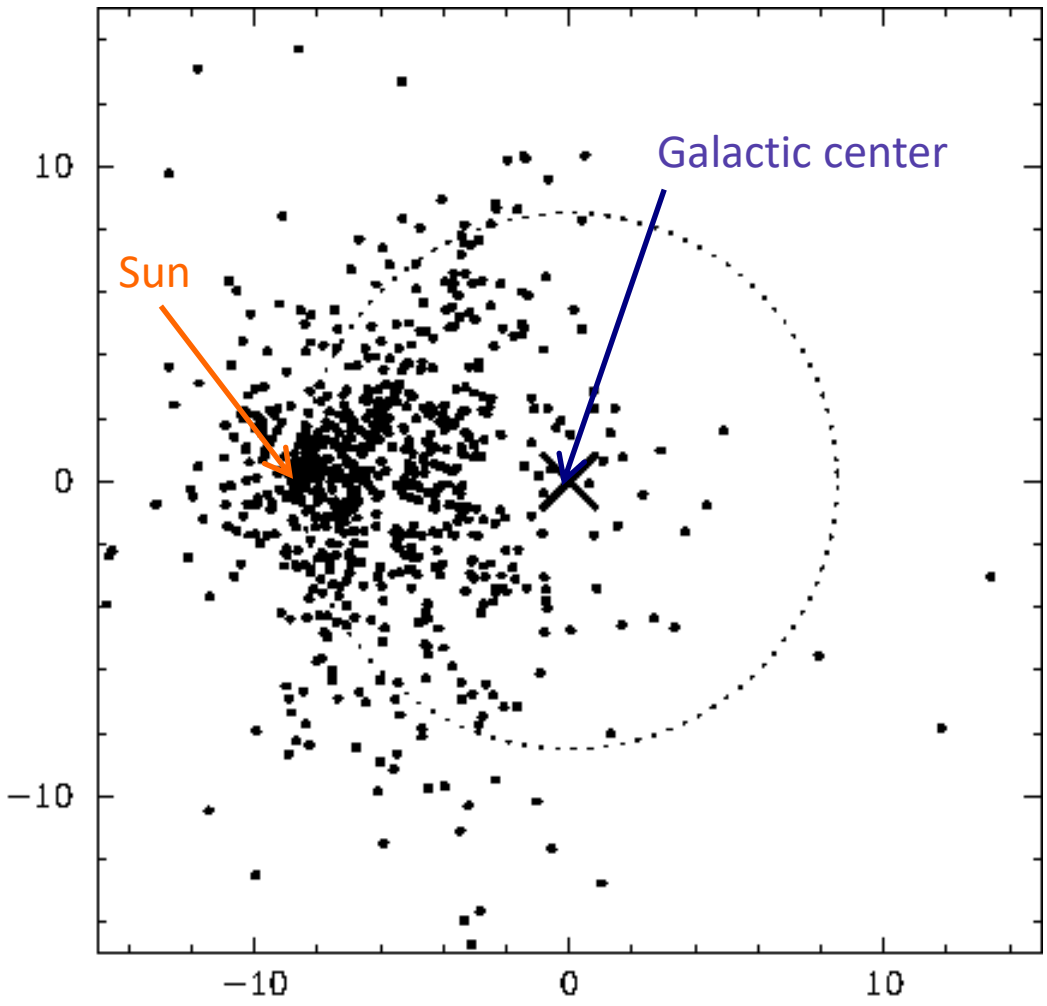

Discovery of radio pulsars with the SKA (Square-Kilometre Array):

Will increase number of known pulsars by a factor 5-10 (Keane et al. 2015)

https://www.youtube.com/watch?v=y07ZAocCjhQ (Swinburne Astronomy Productions)

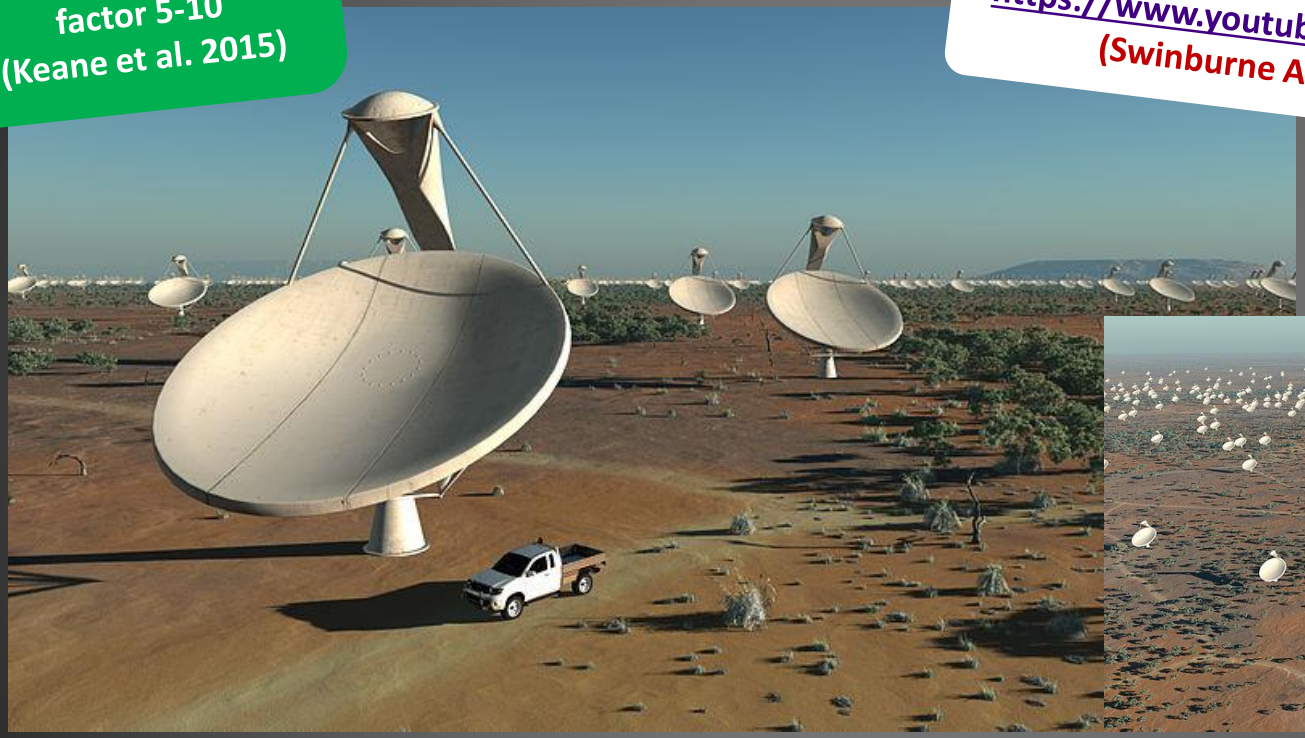

Phase I @ 2023 – Phase II @ 2030 – Frequency range: 50 MHz to 14 GHz.

- SKA-low array (50 – 350 MHz) (dipole antennas)
- SKA-mid array (350 MHz – 14 GHz) (15 m. dish antennas)
- SKA-survey array (350 MHz – 4 GHz) (a compact array of parabolic dishes)

Pulsar pulse profiles

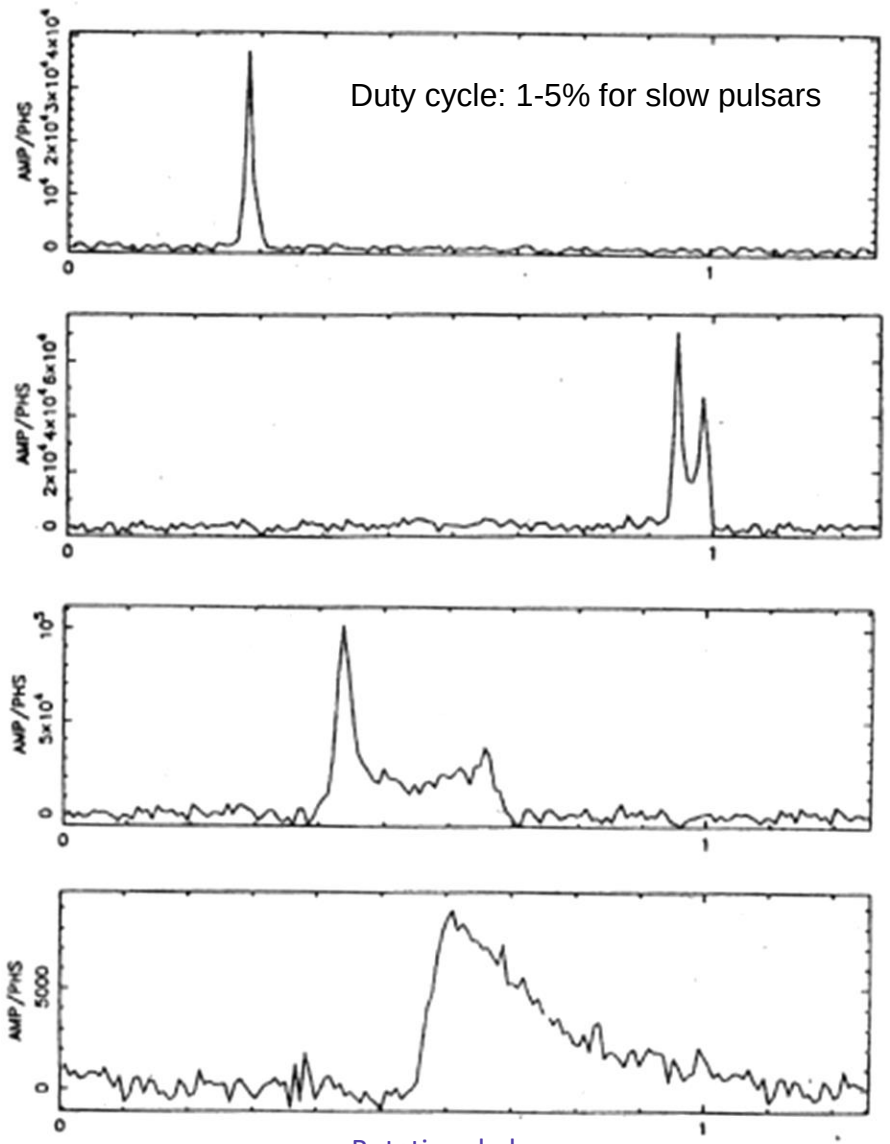

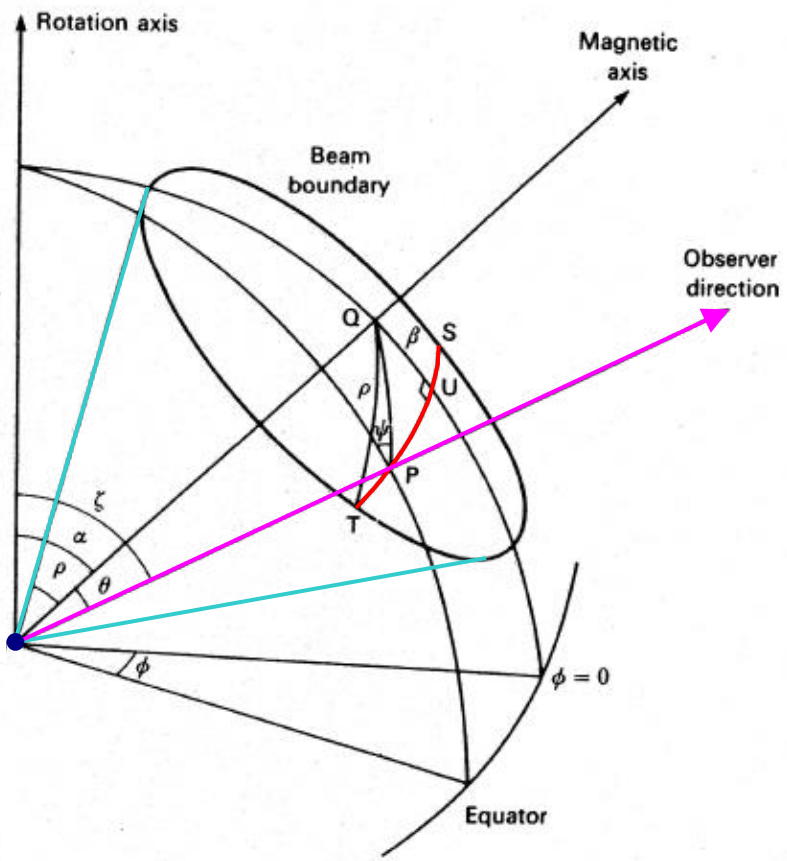

Pulsar pulse profiles

436, 660, 1420 MHz

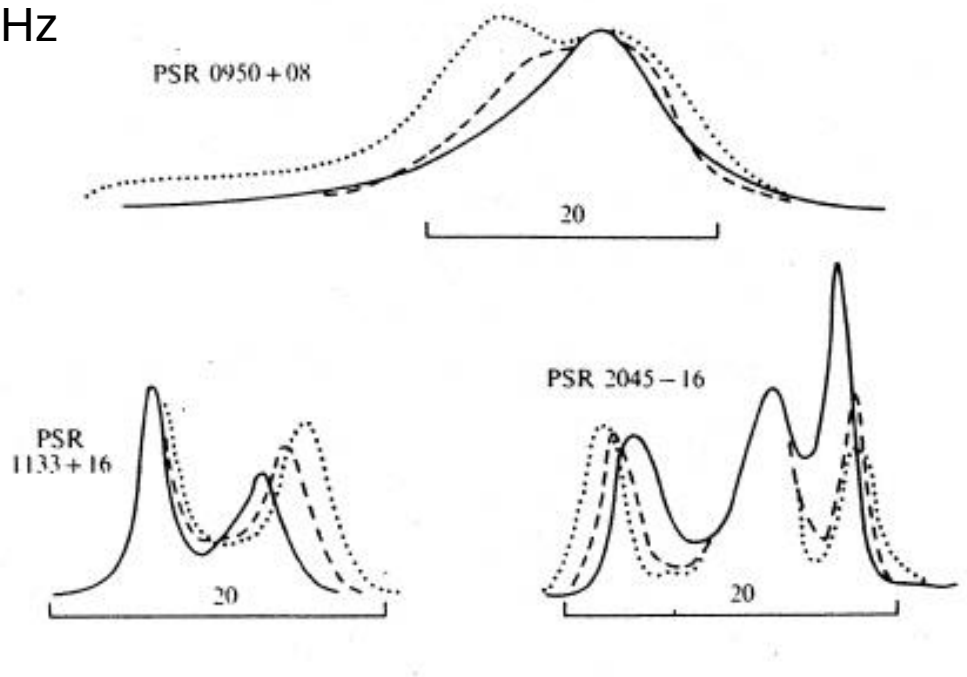

Pulsar pulse profiles

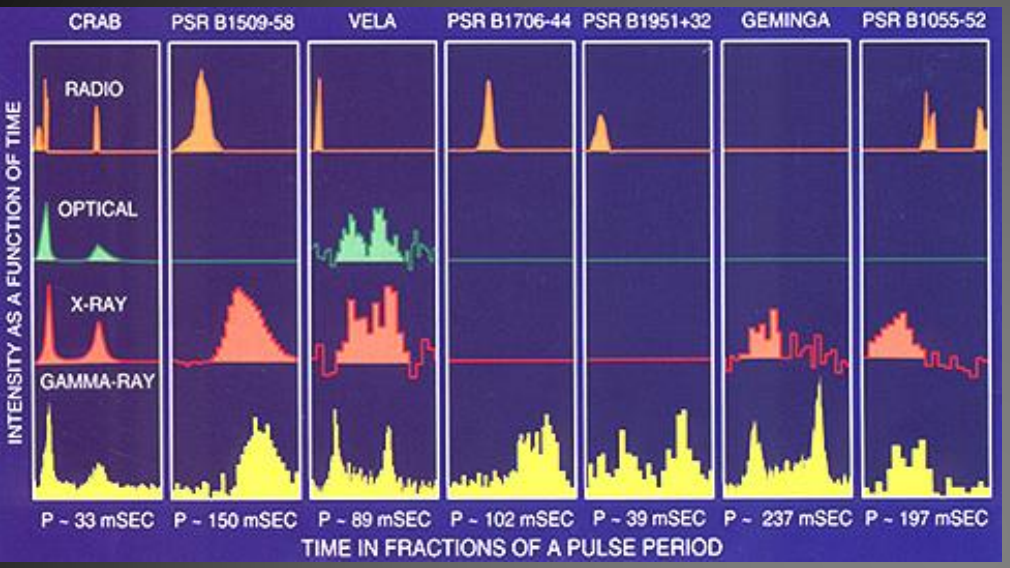

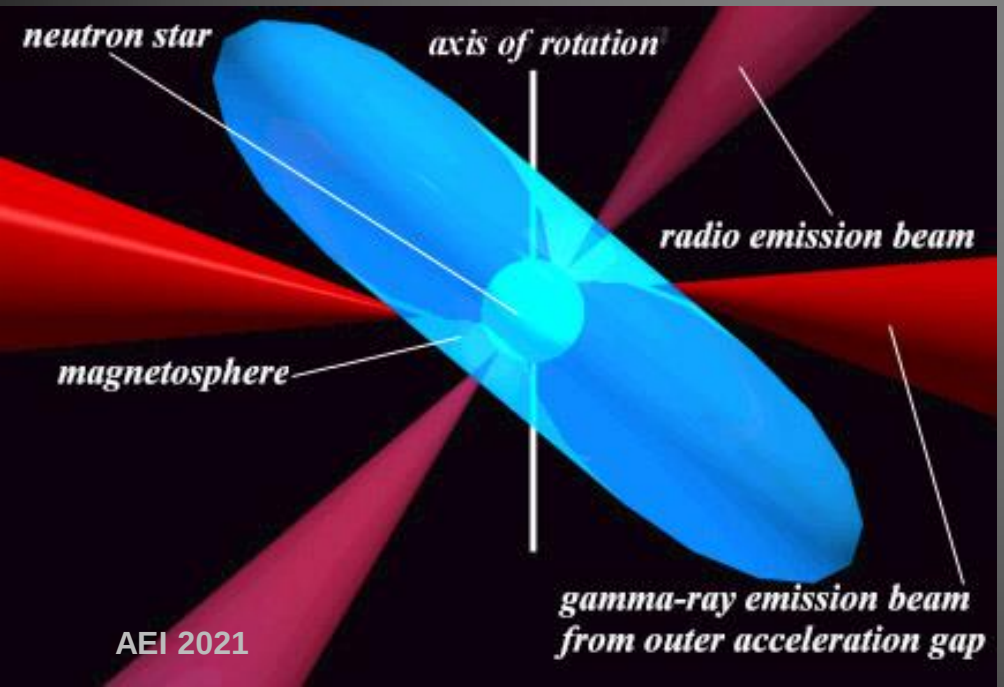

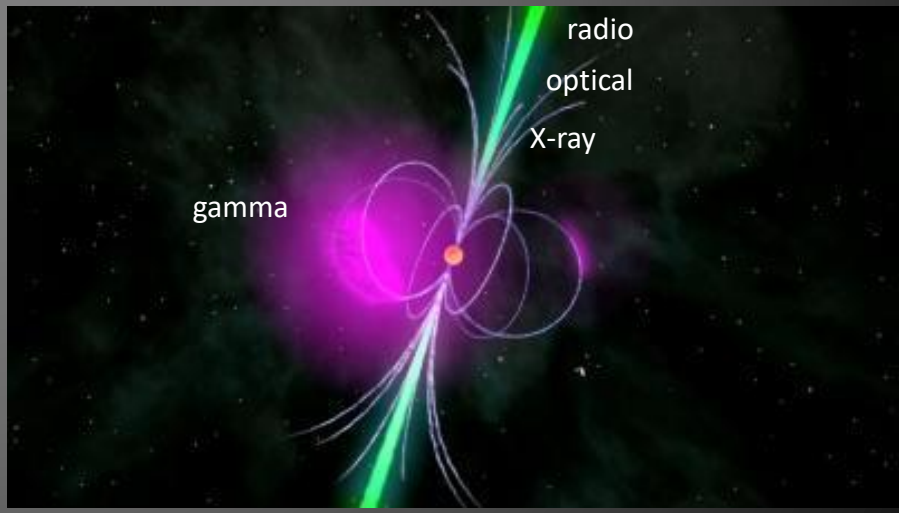

Pulsar pulse profiles

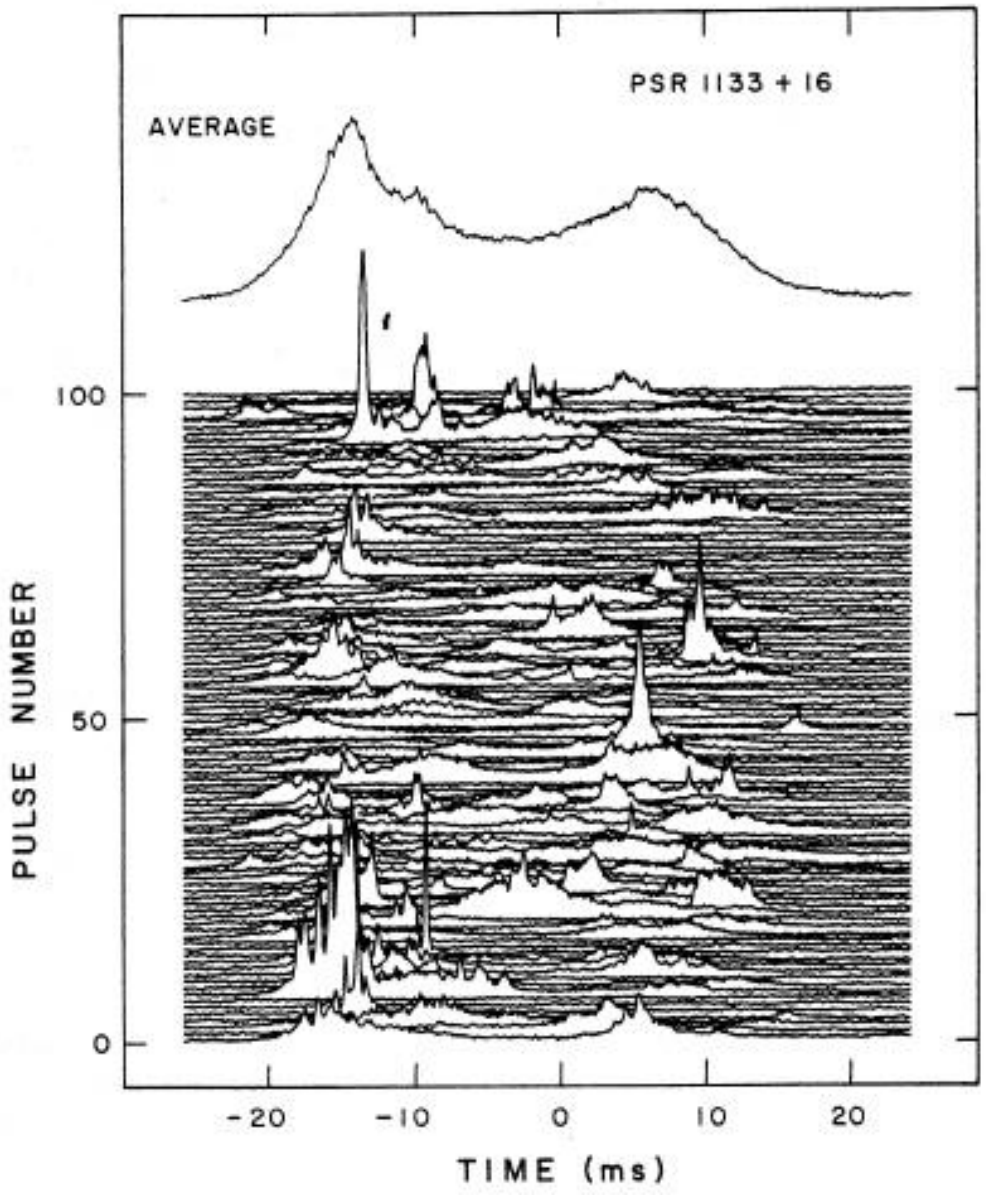

Scintillation (interstellar weather)

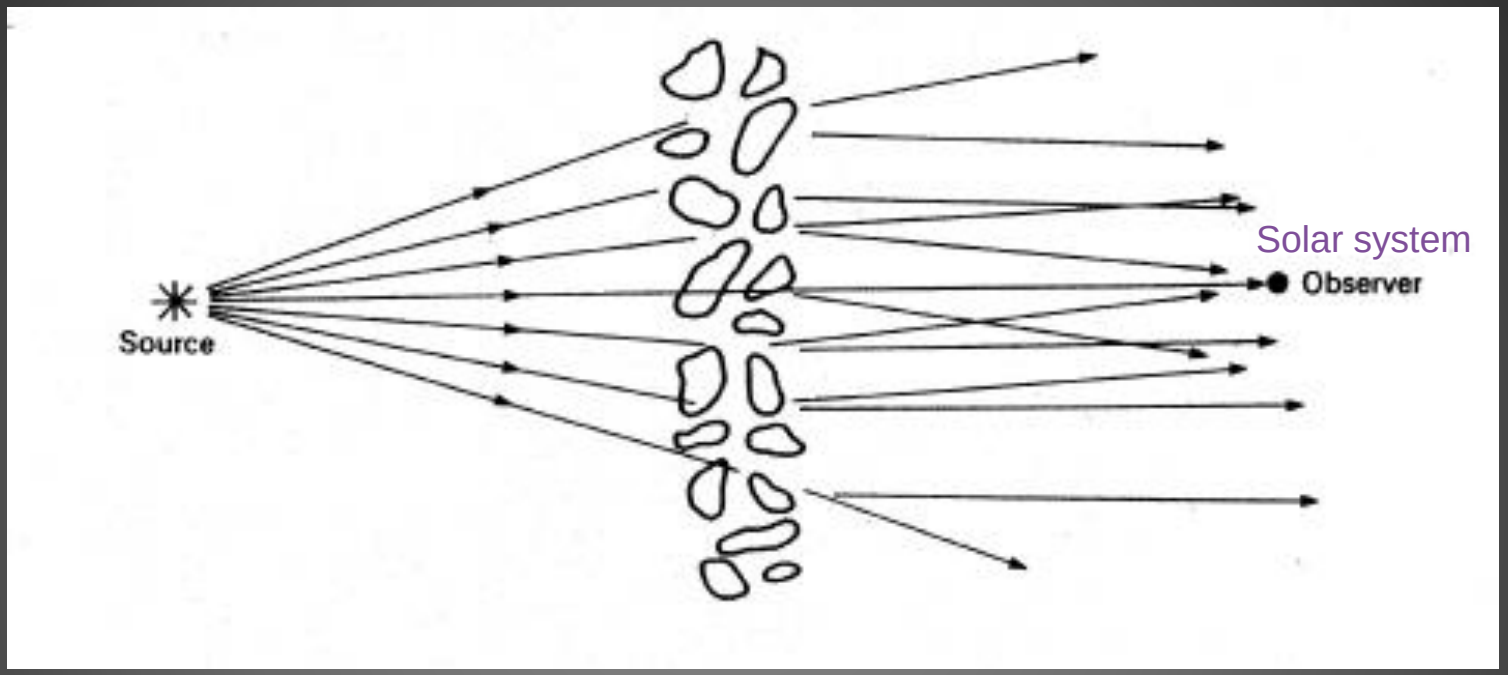

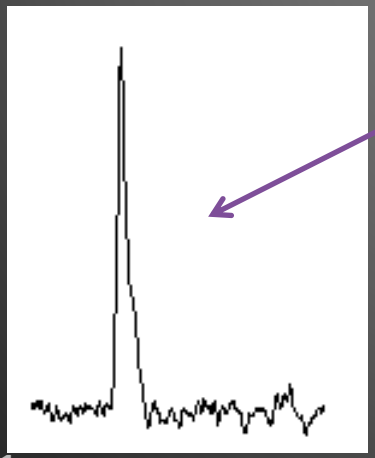

emitted pulse

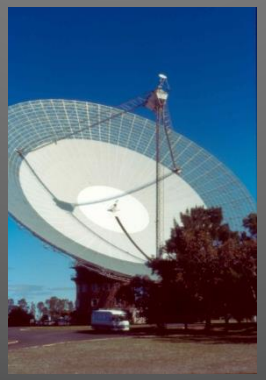

observed pulse

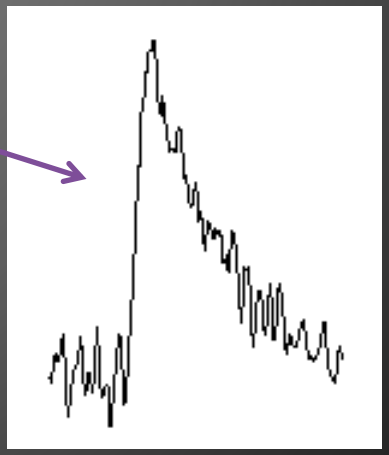

Distance determination of pulsars

452 MHz

256 channels
* 125 kHz

436 MHz
(70 cm)

420 MHz

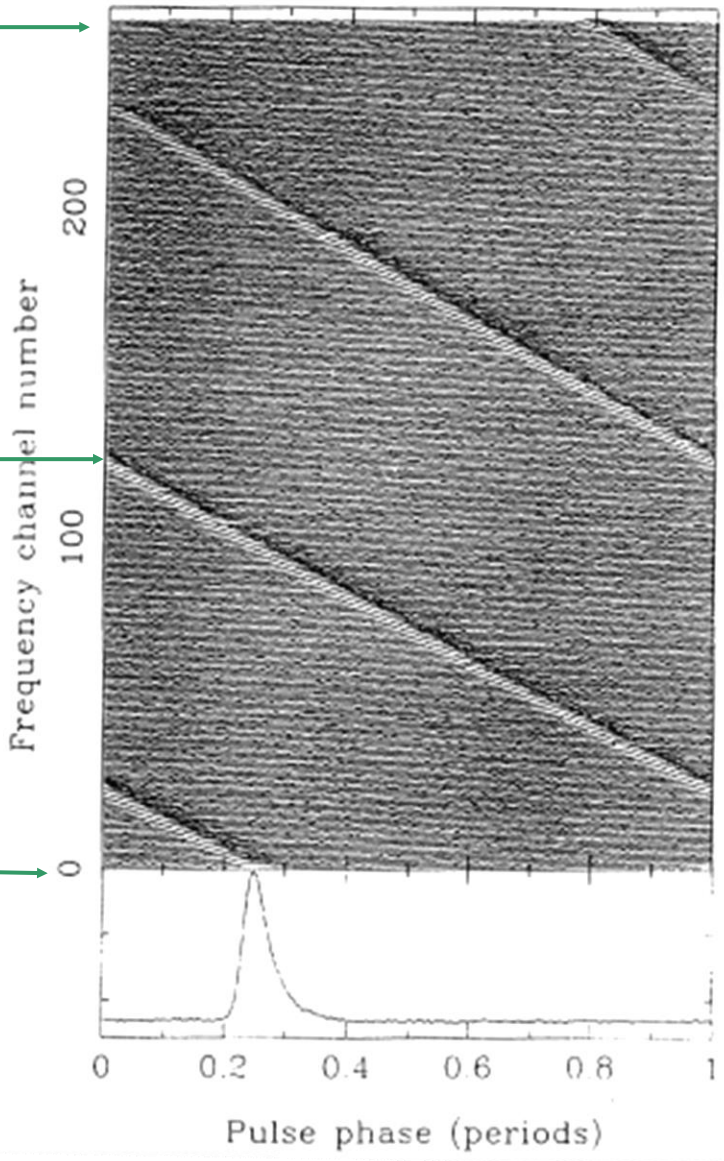

$$\frac{\Delta t_a}{\Delta \omega} = -\frac{4\pi e^2}{m_e c\, \omega^3} DM$$

$$DM = \int_0^L n_e \, dl = \langle n_e \rangle L$$

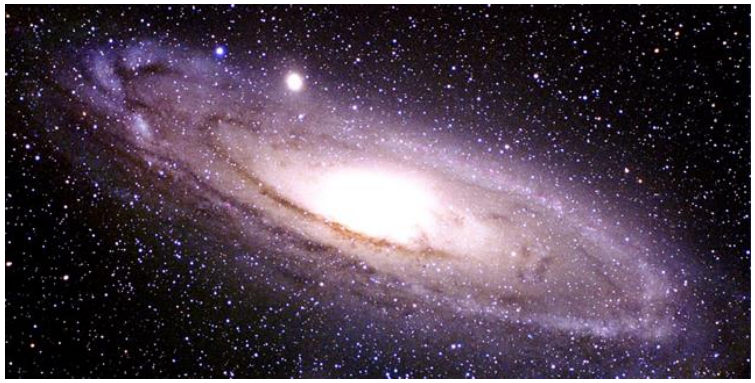

distance α 1/slope

Determination of the stellar wind mass-loss rate of a B-star in the SMC using the binary pulsar PSR J0045-7319 (Kaspi, Tauris & Manchester 1995)

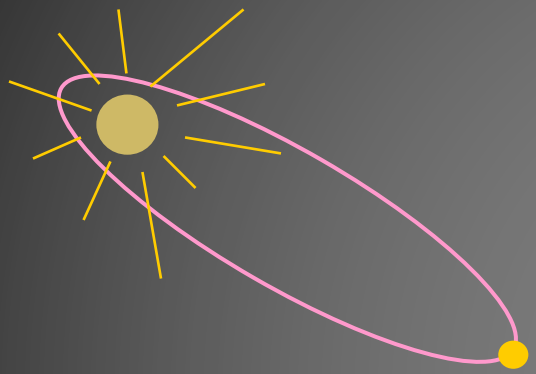

pulsar

$$\frac{dM}{dt} < 3\times10^{-11}\, M_{\odot}\ yr^{-1}$$

- Most accurate method to determine a stellar wind

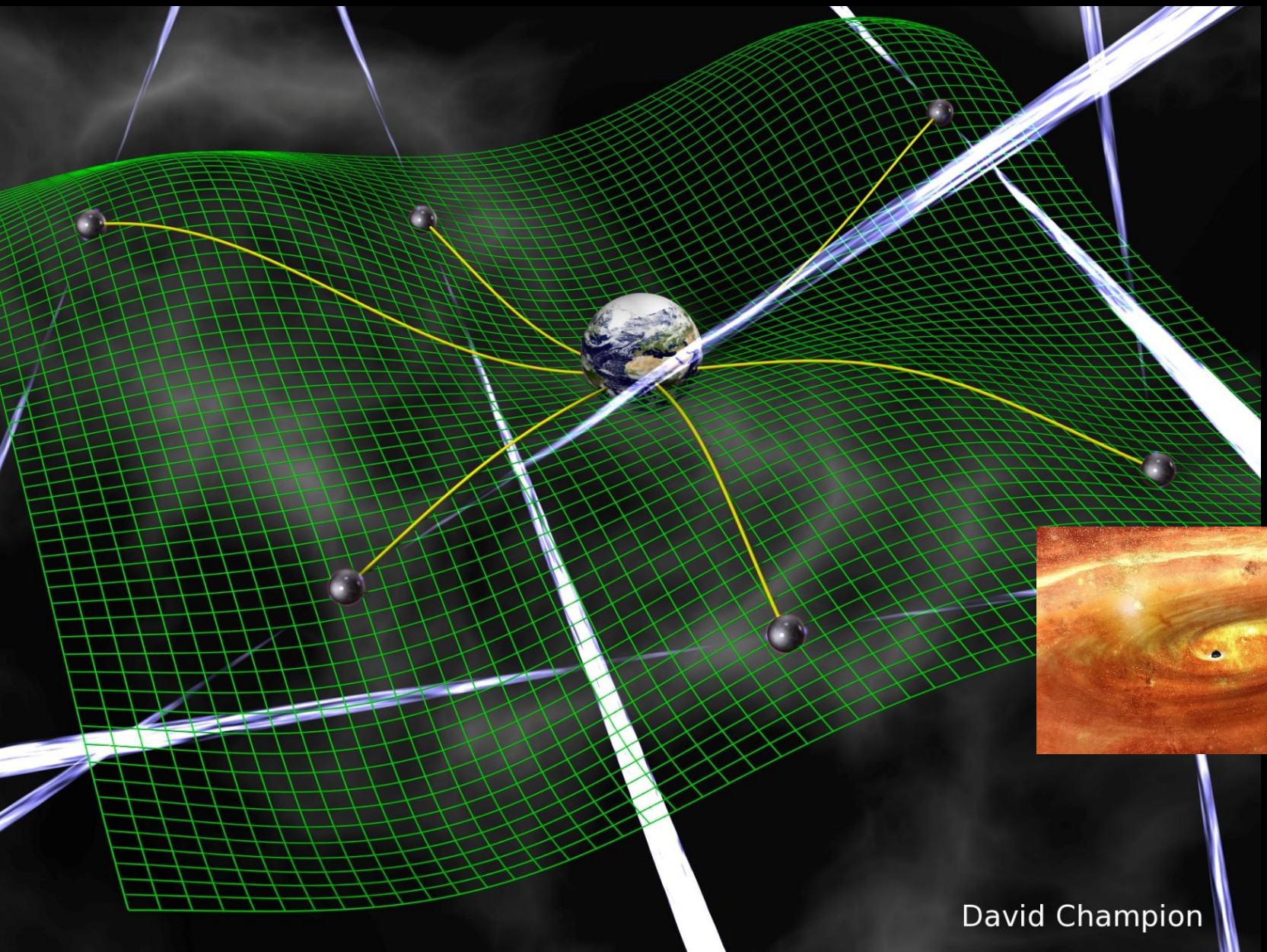

David Champion

PSR J1141–6545

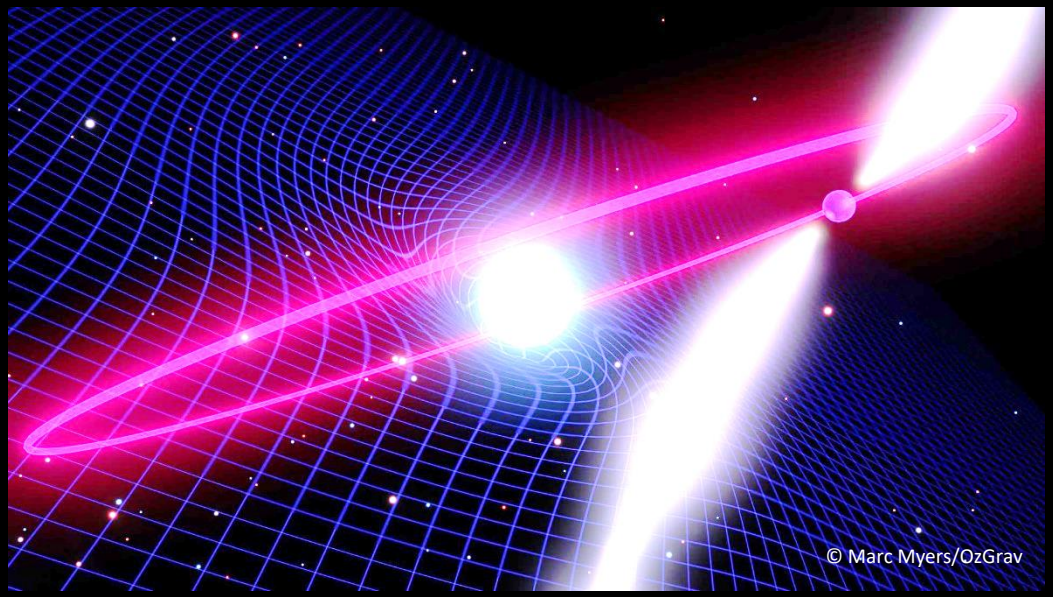

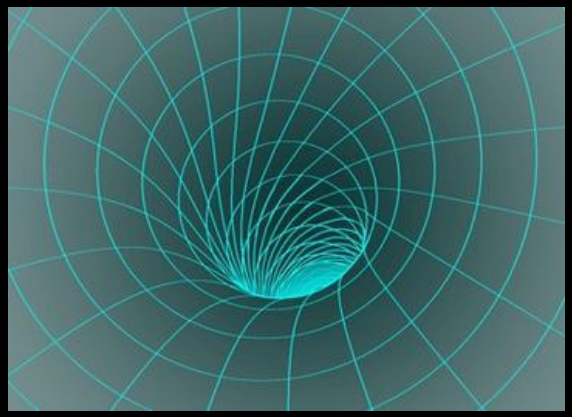

video

https://youtu.be/GOb3MCAg9zM

RESEARCH

REPORT

Science

GRAVITATION

Lense–Thirring frame dragging induced by a fast-rotating white dwarf in a binary pulsar system

V. Venkatraman Krishnan[1,2]*, M. Bailes[1,3], W. van Straten[4], N. Wex[2], P. C. C. Freire[2], E. F. Keane[1,5], T. M. Tauris[2,6,7], P. A. Rosado[1]†, N. D. R. Bhat[8], C. Flynn[1], A. Jameson[1], S. Osłowski[1]

assume an ellipse in flat spacetime

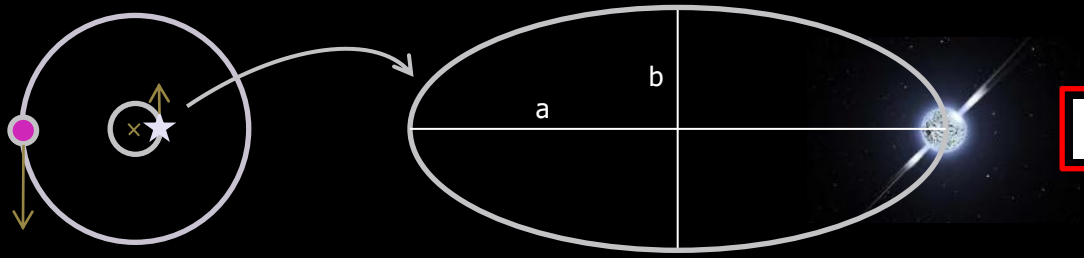

$a - b \approx 6.3\ \mu m$

PSR J1738+0333
Antoniadis et al. (2012)

$ecc = 3.5 \times 10^{-7}$

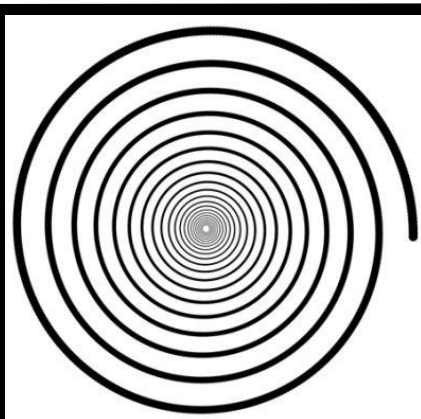

$\Delta a = -30\ \mu m$ per orbit

Tauris & van den Heuvel (2022)

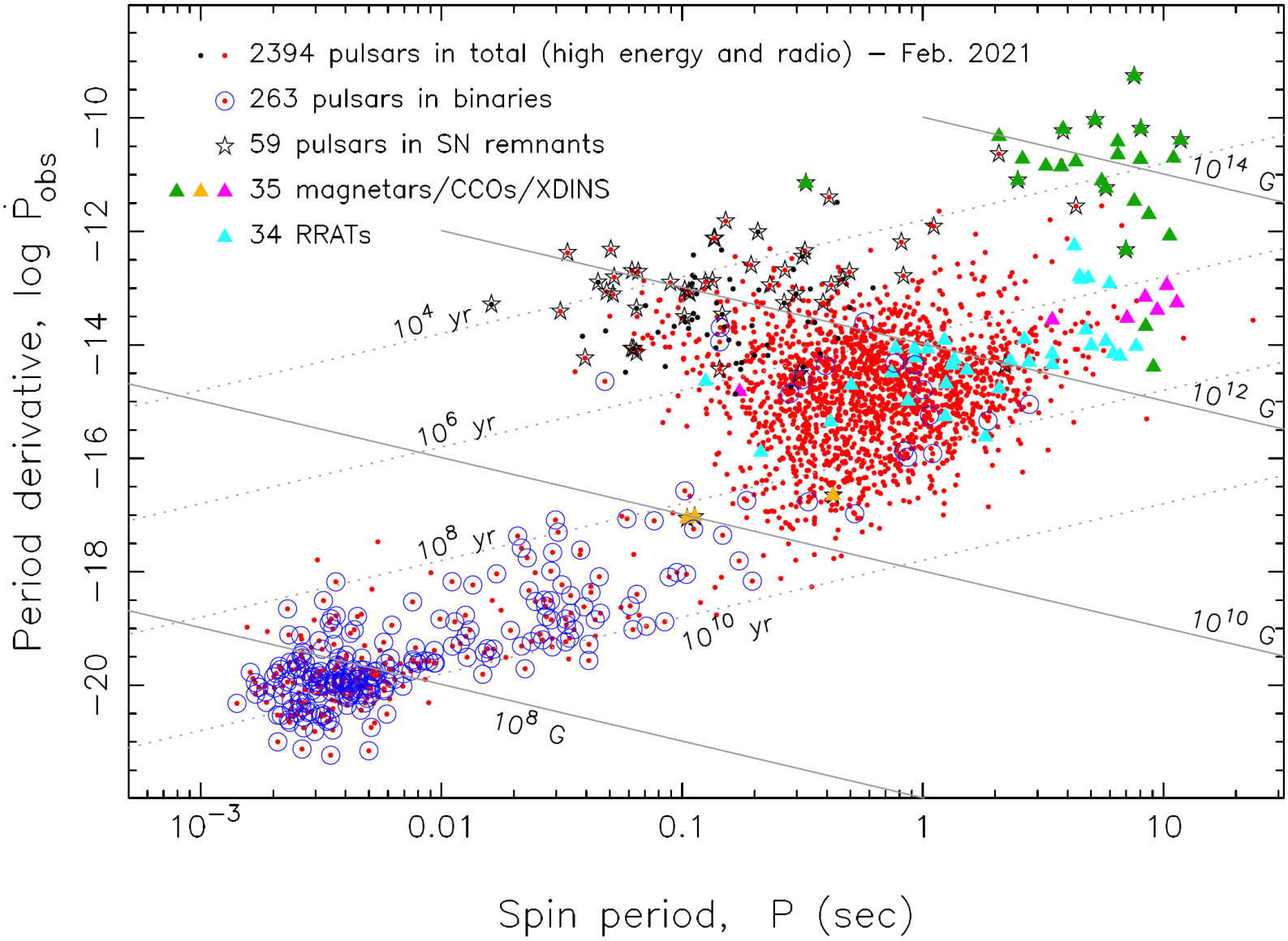

Spin evolution of pulsars

Radio pulsar ($P,\dot{P}$) diagram

The magnetic-dipole model:

$$\dot{E}_{dipole} = -\frac{2}{3c^3}|\ddot{m}|^2$$

$$|\ddot{m}| \sim BR^3\Omega^2\sin\alpha$$

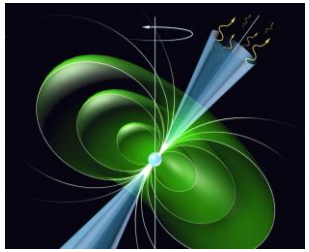

$$E_{rot} = \frac{1}{2} I_{NS}\Omega^2 \quad (\Omega = 2\pi / P)$$

$$\dot{E}_{rot} = I_{NS}\Omega\dot{\Omega}$$

⇕

$$B = \sqrt{\frac{3c^3 I_{NS}}{8\pi^2 R_{NS}^6} P\dot{P}}$$

1

$$\tau \equiv \frac{P}{2\dot{P}}$$ Characteristic age

Active pulsar lifetime: 10-50 million yr

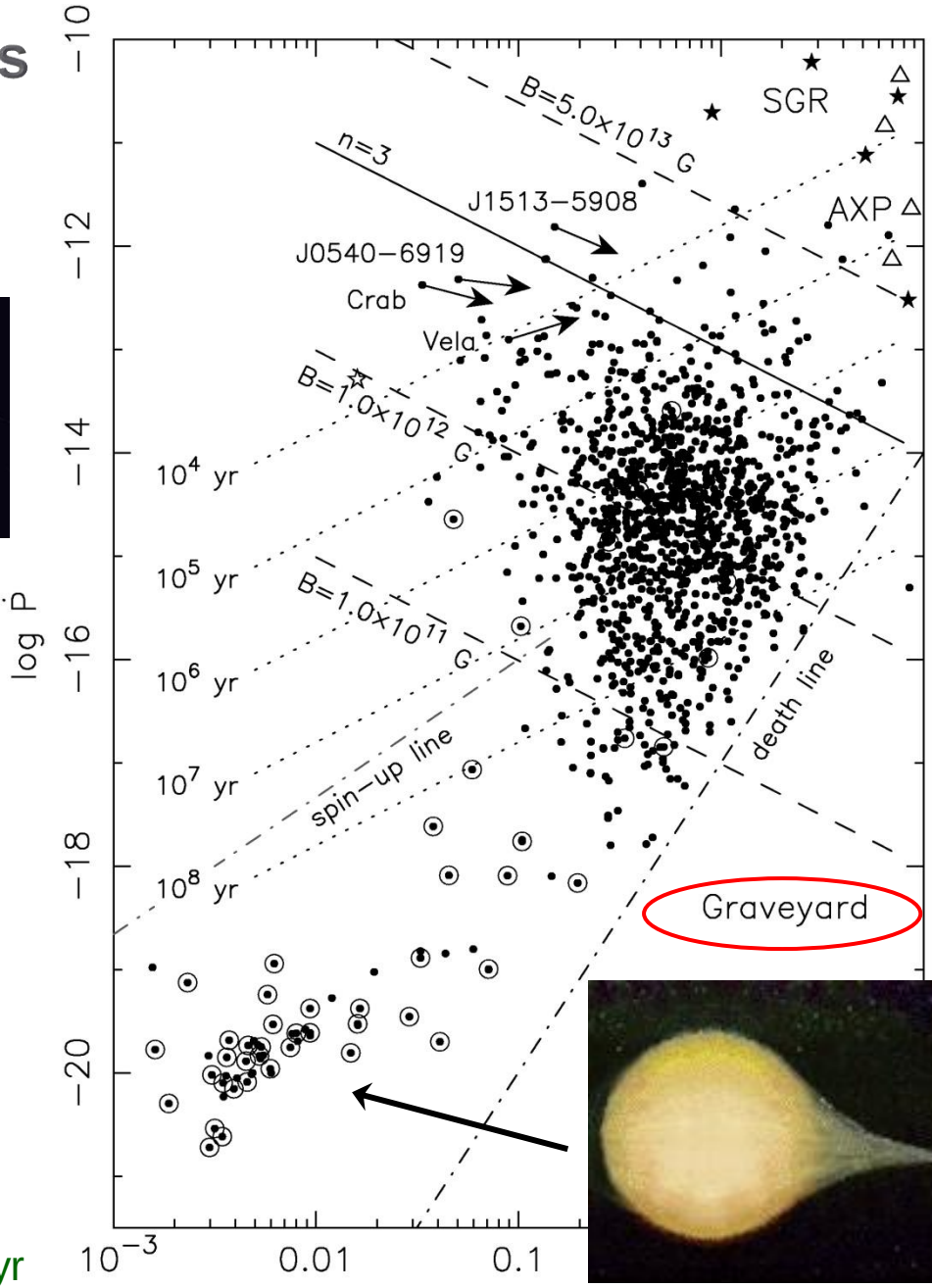

Acceleration of charged particles ⇨ electromagnetic waves:

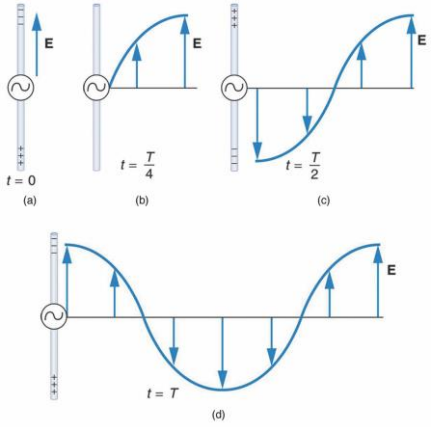

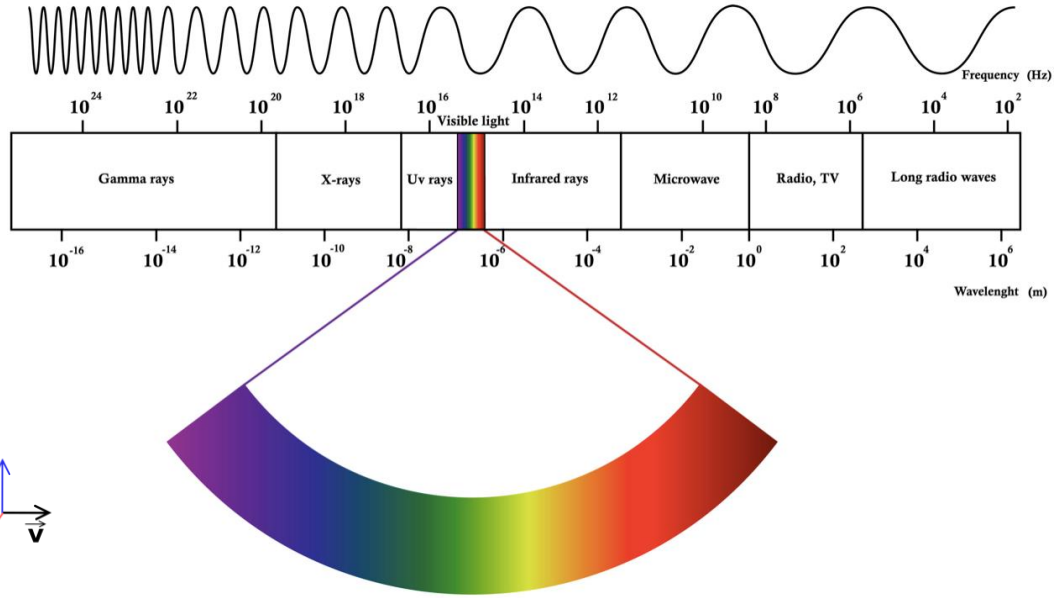

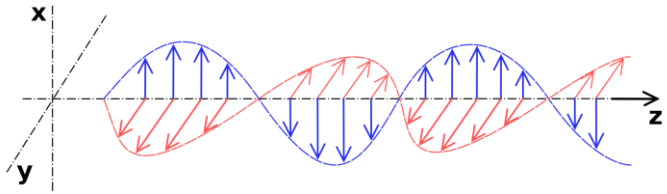

Acceleration of masses ⇨ gravitational waves: (approximately true)

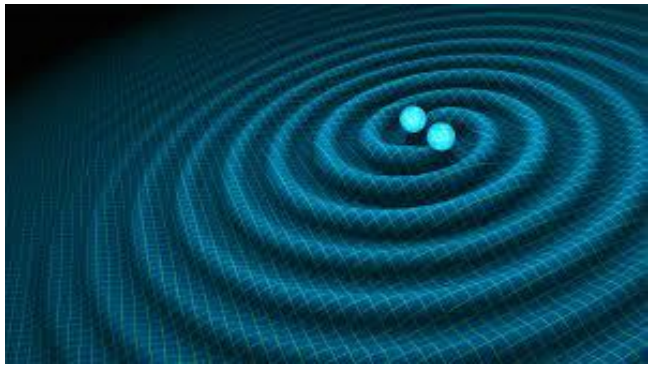

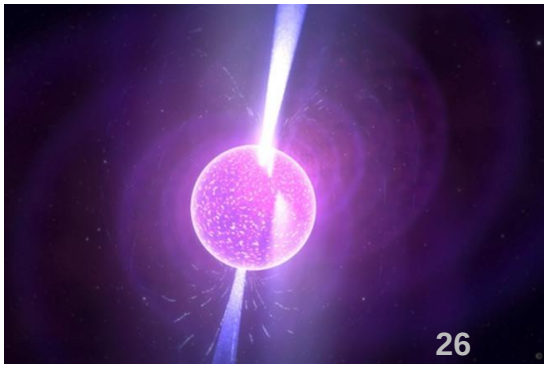

A time-varying **quadrupole moment*** gives rise to emission of gravitational waves with an **amplitude**:

$$h_{\mu\nu} \approx \frac{2G}{c^4 d} \ddot{Q}_{\mu\nu}$$

$\ddot{Q}_{\mu\nu}$ → quadrupole moment

d → distance to source

(Newtonian quadrupole-approximation)

* An asymmetric distribution of mass with respect to the spin axis:

☐ no gravitational waves

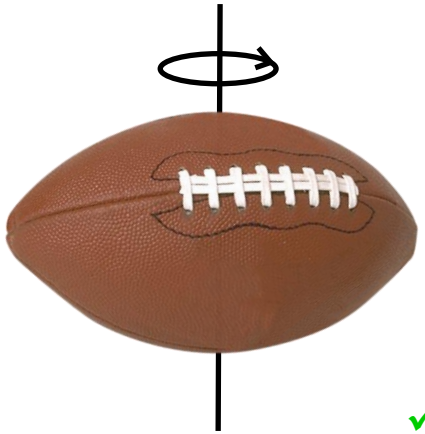

✓ gravitational waves

$$L_{GW} = \frac{dE}{dt} = \frac{G}{5c^5} \langle \dddot{Q}_{\mu\nu} \, \dddot{Q}_{\mu\nu} \rangle$$

A rough estimate:

$$Q \sim MR^2 \quad \Rightarrow \quad \dddot{Q} \sim \frac{MR^2}{T^3} \sim \frac{Mv^3}{R}$$

where (M,R,T,v) are characteristic values for the source

1 mm "mountain" on a neutron star:

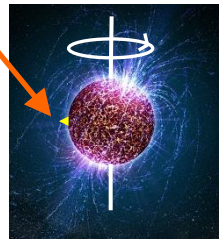

$M = 1.4\ M_\odot$
$R = 10$ km, $\Delta r = 1$ mm
$\Omega = 2\pi\nu = 1000$ rad s^{-1}

$I \sim MR^2$

$L_{GW} = 10^{36}$ erg s^{-1}

steel cylinder:

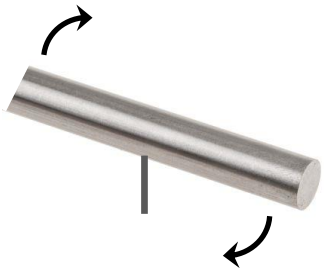

$M = 140.000$ kg
$R = 20$ m (dia=1 m)
$\nu = 300$ m s^{-1}

$L_{GW} = 10^{-24}$ erg s^{-1}

$$L_{GW} \equiv \frac{|dE|}{dt} = \frac{32G}{5c^5} I^2 \varepsilon^2 \Omega^6$$

$$\varepsilon = \frac{a-b}{(a+b)/2} \approx \frac{\Delta r}{R}$$

ellipticity perpendicular to spin axis

a factor $\sim 10^{60}$ in difference!!!

Resonance mass detectors

Auriga, Padova → 2009

Joseph Weber 1960s

Spin evolution of pulsars

Self study!

(2) $\dot{\Omega} = -k\,\Omega^n$ the deceleration law, (3) $n = \dfrac{\ddot{\Omega}\Omega}{\dot{\Omega}^2}$ is the braking index

Differentiate Eq.(2)

$n = 3$ pure dipole

$n = 5$ pure gravitar (only spin-down by gravitational wave radiation)

true age of pulsars: (4) $t = \dfrac{P}{(n-1)\dot{P}}\left[1-\left(\dfrac{P_0}{P}\right)^{n-1}\right]$

Integrate Eq.(2)

Characteristic age

$\Rightarrow$ (5) $\tau \equiv \dfrac{P}{2\dot{P}}$, for $P \gg P_0,\ n = 3$

$\dot{E}_{dipole} = -\dfrac{2}{3c^3}|\ddot{m}|^2$ $\quad |\ddot{m}| \sim BR^3\Omega^2\sin\alpha$

second derivative of magnetic moment

$\dot{E}_{gw} = -\dfrac{32}{5}\dfrac{G}{c^5}I^2\varepsilon^2\Omega^6$

$\dot{E}_{rot} = I\Omega\dot{\Omega} = \dot{E}_{dipole} + \dot{E}_{plasma} + \dot{E}_{gw}$

$\varepsilon = \dfrac{a-b}{(a+b)/2}$

ellipticity (asymmetry $\perp$ rotation axis)

For example:

(6) $B(t) = B_0 \cdot e^{-t/\tau_D}$ Insert into Eq.(1) and integrate will yield Eq.(7)

(7) $P(t)^2 = P_0^2 + B_0^2\,\tau_D\left(1-e^{-2t/\tau_D}\right)\cdot\dfrac{1}{k^2}$ (8) $t \simeq \dfrac{\tau_D}{2}\ln\left(\dfrac{2\tau}{\tau_D}+1\right)$ $\quad \tau \equiv \dfrac{P}{2\dot{P}}$

Combine Eqs.(1), (5), (6) and (7)

Spin evolution of pulsars

Self study!

(2) $\dot{\Omega} = -k\Omega^n \quad \Rightarrow \quad n = \frac{\ddot{\Omega}\Omega}{\dot{\Omega}^2} = 2 - \frac{\ddot{P}P}{\dot{P}^2} \quad \wedge \quad P^{n-2}\dot{P} = const$

Given $(P_0, \dot{P}_0, n = const, t)$ we can calculate $P(t)$ and $\dot{P}(t)$:

(9) $P(t) = P_0\left(1 + (n-1)\frac{\dot{P}_0}{P_0}\,t\right)^{\frac{1}{n-1}} \qquad \dot{P}(t) = \dot{P}_0\left(\frac{P(t)}{P_0}\right)^{2-n}$

substitute $P = 2\pi/\Omega$ into Eq.(2)
and integrate yields Eq.(9) (cf. Lazarus et al. (2014) for evolutionary tracks)

Slope in the $(P, \dot{P})$ – diagram: $2 - n$

$B = const$: $\dot{P} \propto \frac{1}{P} \quad \Rightarrow \quad -1$

$\tau = const$: $\dot{P} \propto P \quad \Rightarrow \quad +1$

death line: $\Delta\varphi \propto B / P^2 \quad \Leftrightarrow \quad \dot{P} \propto P^3 \quad \Rightarrow \quad +3$

Electrostatic potential across polar caps

spin-up line: $P_{eq} \propto B^{6/7} \quad \Leftrightarrow \quad \dot{P} \propto P^{4/3} \quad \Rightarrow \quad +4/3$

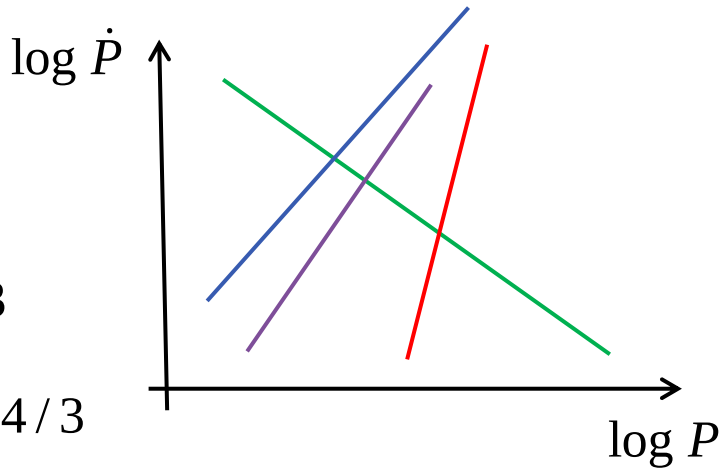

Spin evolution of pulsars

Tauris & Konar (2001)

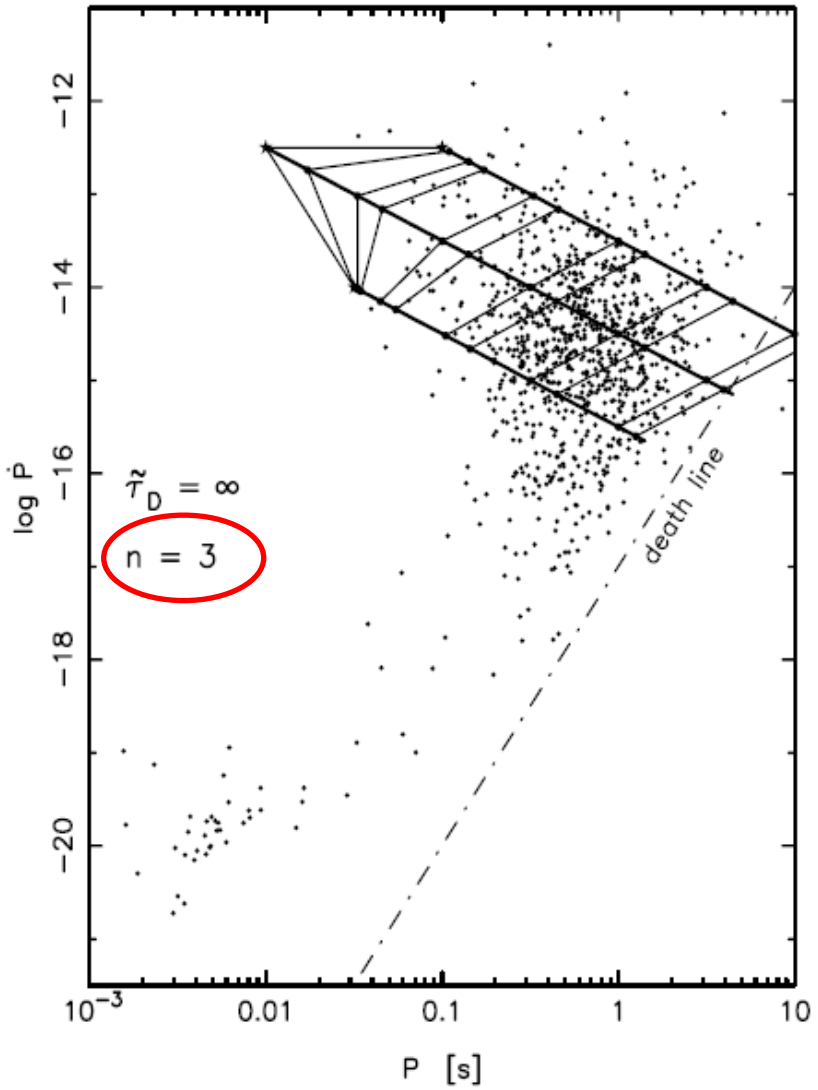

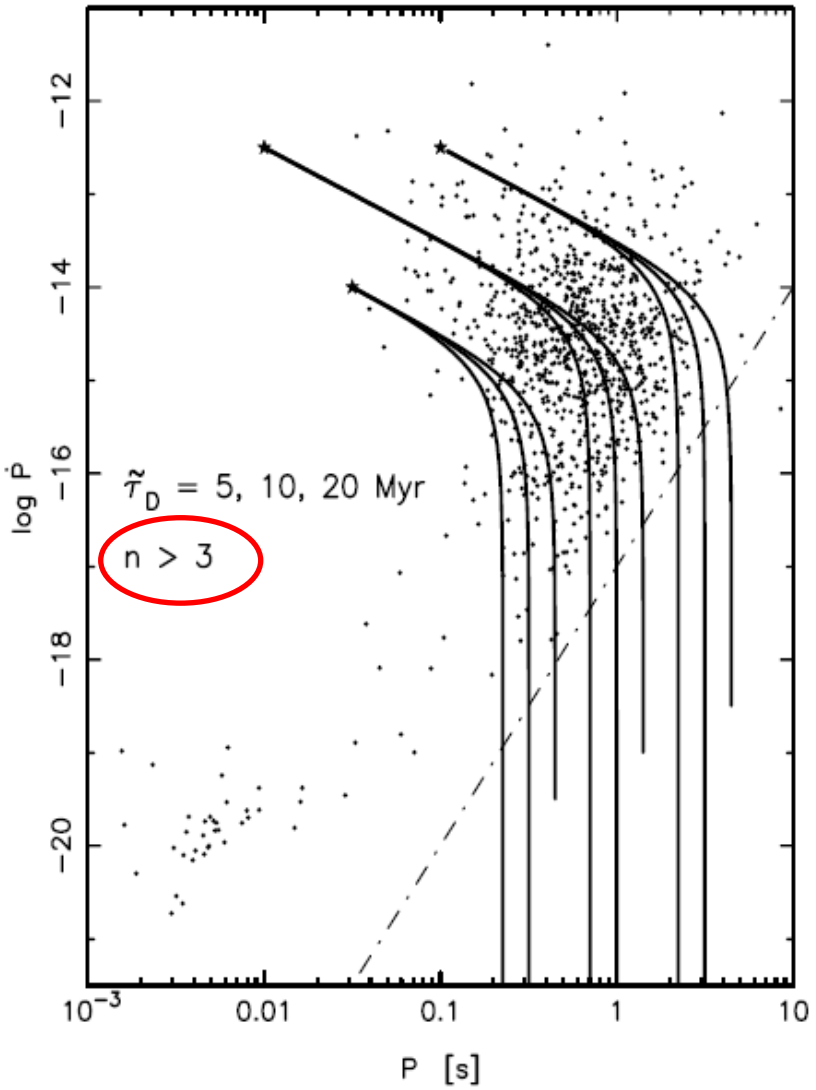

B-fields

B-field decay in neutron stars, via crustal ohmic dissipation and diffusion, and its dependence on input physics.

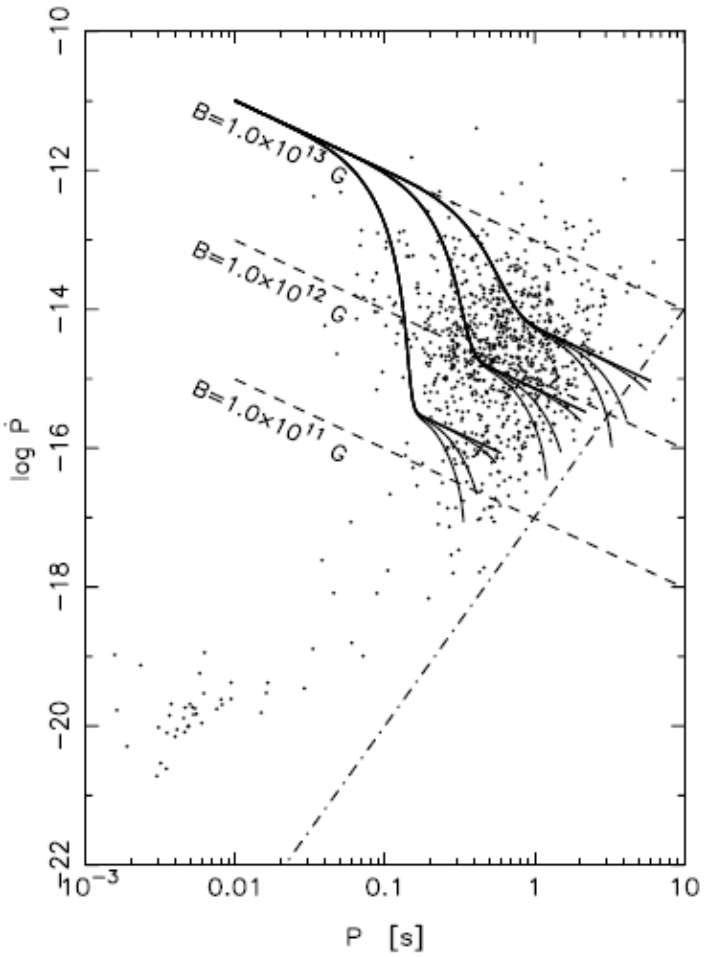

Fig. 6. Evolutionary tracks in the $(P, \dot{P})$ diagram assuming $P_0 = 10$ ms and $\dot{P}_0 = 10^{-11}$ ($B_0 = 10^{13}$ G) calculated from $\rho_0 = 10^{11}$–10^{13} g cm^{-3} and $Q = 0$–0.10 – see text. Each track was followed for 100 Myr. The small dots represent data.

$$\frac{\partial \vec{B}}{\partial t} = \nabla \times \left(\vec{v} \times \vec{B}\right) - \frac{c^2}{4\pi} \nabla \times \left(\frac{1}{\sigma} \times \nabla \times \vec{B}\right)$$

$$B = \sqrt{\frac{3c^3 I_{NS}}{8\pi^2 R_{NS}^6} P\dot{P}}$$

A.2. The field evolution equation

We use the form of $B(r, \theta, \phi)$ given by Eq. (A.3) to cast Eq. (A.7) in terms of the Stokes' stream function.
I. The left hand side:

$$\frac{\partial \boldsymbol{B}}{\partial t} = \frac{\partial \nabla \times \boldsymbol{A}}{\partial t} = \nabla \times \frac{\partial}{\partial t} \left[\frac{g(r,\theta)\, \sin\theta}{r}\right] \hat{\phi}. \qquad \text{(A.10)}$$

II. The right hand side:

$$\nabla \times \left[\frac{1}{\sigma} \nabla \times \boldsymbol{B}\right] =$$

$$\nabla \times \left[\frac{1}{\sigma} \nabla \times \left(\frac{2\cos\theta\, g(r,t)}{r^2}\, \hat{r} - \frac{\sin\theta}{r} \frac{\partial g(r,t)}{\partial r}\, \hat{\theta}\right)\right] =$$

$$\nabla \times \left[-\frac{1}{\sigma} \frac{\sin\theta}{r} \left(\frac{\partial^2 g(r,t)}{\partial r^2} - \frac{2g(r,t)}{r^2}\right) \hat{\phi}\right]. \qquad \text{(A.11)}$$

Incorporation of the expressions (A.10) and (A.11) in Eq. (A.7) then leads to:

$$\frac{\partial g(r,t)}{\partial t} = \frac{c^2}{4\pi\sigma} \left(\frac{\partial^2 g(r,t)}{\partial r^2} - \frac{2g(r,t)}{r^2}\right). \qquad \text{(A.12)}$$

B-fields

More advanced calculations by Vigano et al. (2013)

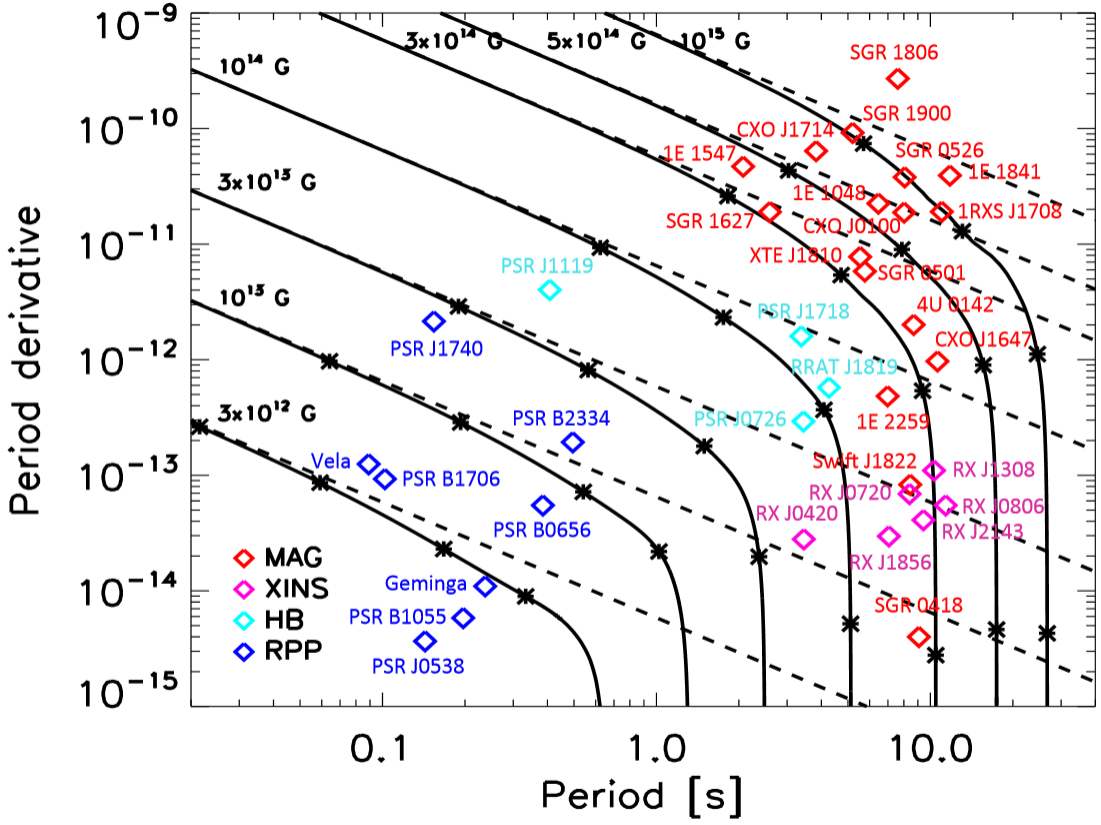

Magnetars

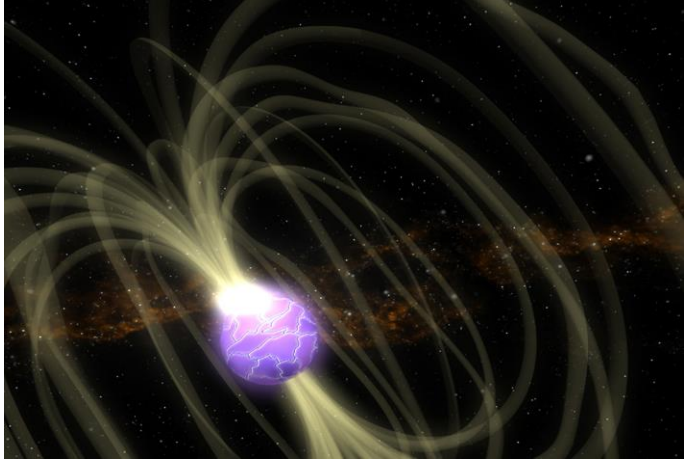

Reviews: Turolla, Zane and Watts (2015)
Kaspi & Beloborodov (2017)

A magnetar is a type of neutron star with an extremely high B-field, the decay of which powers the high-energy emission of anomalous X-ray pulsars (AXPs) and soft gamma-ray repeaters (SGRs).
Duncan & Thompson & (1992) developed the theory to explain these objects.

Support for this extreme B-field picture comes from:

1) Location in P-P_{dot} diagram
2) Cannot be radio pulsars b/c $L_X >> \dot{E}_{rot}$
3) Cannot be X-ray binaries b/c absence of Doppler modulation in timing data
4) Cannot be neutron stars accreting from a fall-back disk b/c of detection of flares
5) Bursts can be explained by magnetic giant flares

Magnetars are detected both as persistent (quiescent) sources and burst sources.

There are currently 30 known magnetars: 16 SGRs and 14 AXPs according to McGill SGR/AXP online catalogue:
https://www.physics.mcgill.ca/~pulsar/magnetar/main.html
with various burst, transient and persistent properties

New magnetar
ATel# 13559
March 17, 2020

Examples of magnetars (from Silvia Zane)

	Hosts	P (s)	B (10^{14}G)	kT(keV) / Γ	L (10^{33} erg/s) (0.2-10keV)	comments
4U 0142+61		8.7	1.3	0.46 / 3.4	72	hard X
RXS J1708-4009		11	4.7	0.44 / 2.4	80-190	hard X
1E 1841-045	Kes 73	11.8	7.1	0.44 / 2.0	110	hard X
1E 2259+586	CTB 109	7.0	0.6	0.41 / 3.8	17 - 159	~ transient/hard X
CXO J0100-72	in SMC	8.0	3.9	0.38 / 2.0	200	
1E 1048-5937		6.4	3.9	0.63 / 2.9	5.3 - 250	~ transient
1E 1547-5408		2.0	2.2	0.52 / 2.9	2.6 - 170	transient/radio
XTE 1810-197		5.5	2.9	0.67 / 3.7	5 - 260	transient/radio
CXO 1647-4552	in Wes1	10.6	1.5	0.68/2.0	1-130	transient
AX J1845-0258	G29.6+0.1	7.0	-	/ 4.6	5 - 120	transient
SGR 1900+14	OB	5.2	5.7	0.43 / 2.0	200 - 350	GF/hardX
SGR 1806-20	OB	7.5	7.8	0.6 / 1.4	320 - 540	GF/hardX/outburst
SGR 0526-66	in LMC	8.0	7.4	0.53 / 3.1	260	GF/?
SGR 1627-41	G337.0-0.1?	6.4 ?	-	/ 2.9	4 - 100	outburst

Magnetars

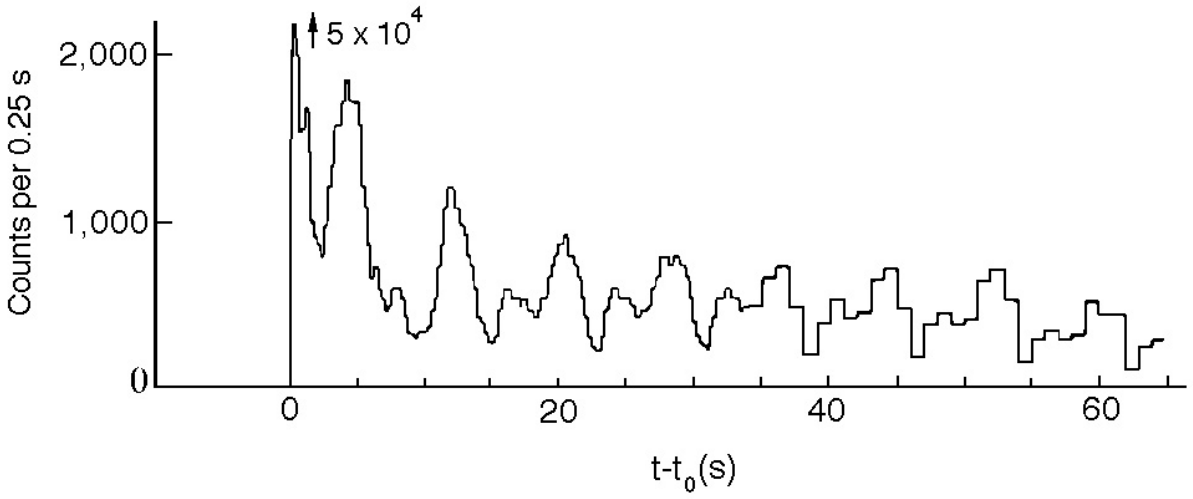

The famous March 5, 1979 event
(the largest burst of gamma-rays ever detected)
Notice, the 8.0 sec cycle (spin period of NS).

16 additional small bursts seen between 1979–1983
and since then no burst have been detected.

The source was located in an LMC SN remnant

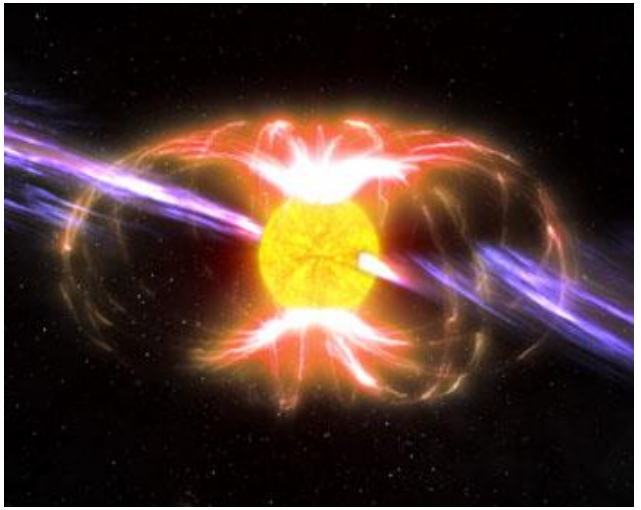

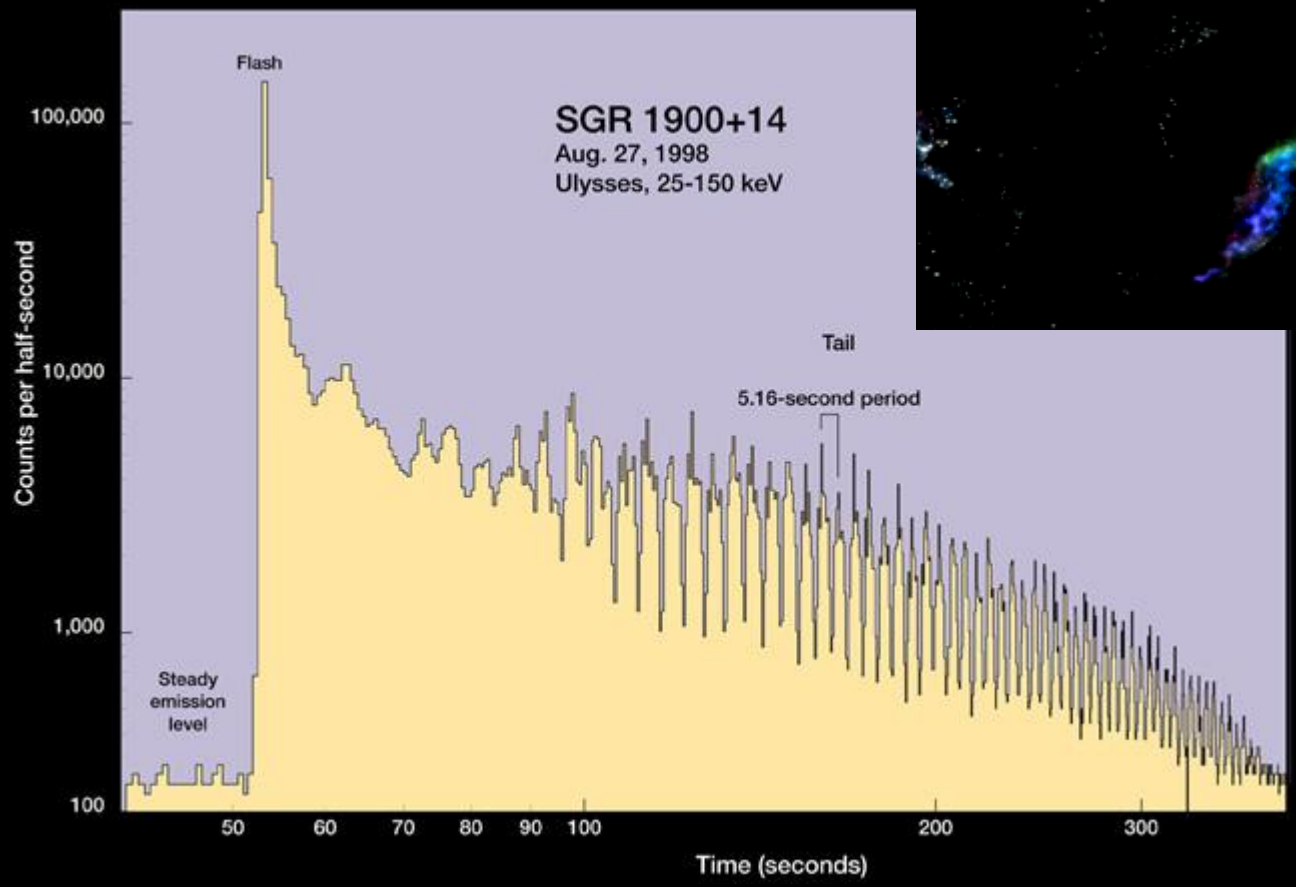

Impact on Earth!

Another famous giant flare (burst) is the August 27, 1998 event (most intense flux of gamma-ray ever detected)

Magnetars

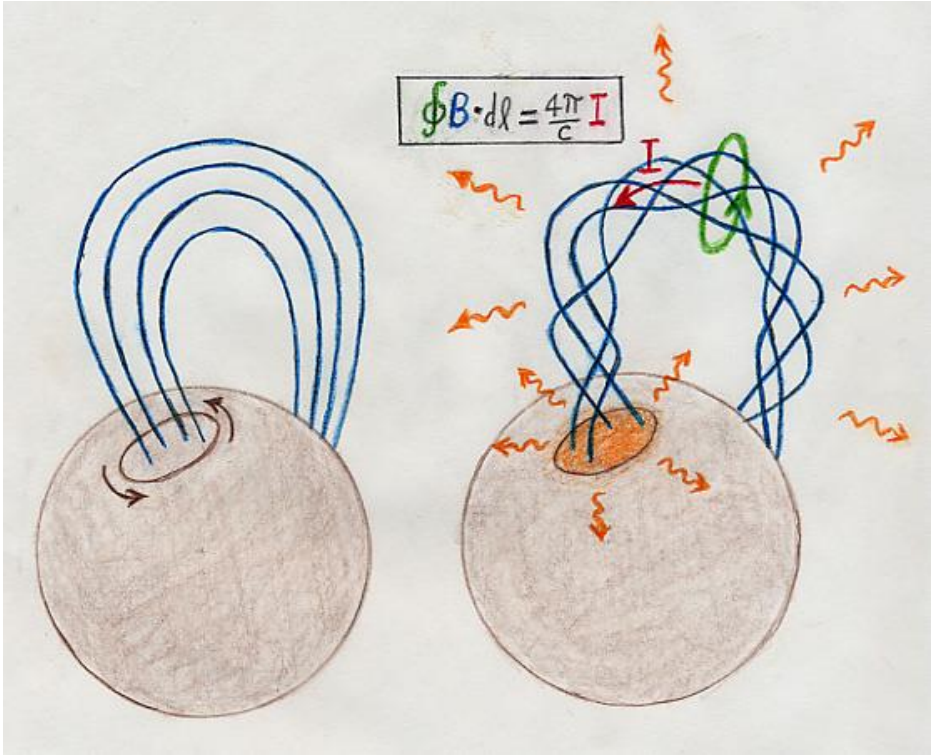

A magnetic twist gives rise to
X-ray emissions from a magnetar.

Robert C. Duncan, University of Texas at Austin

Twisted B-fields support excess currents in the magnetosphere.
Detection of resonant cyclotron scattering reveals the B-field strengths.

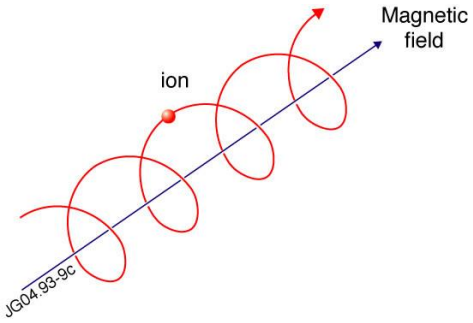

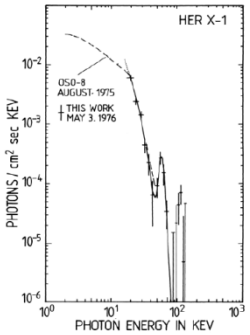

$$E_{cyclotron}^{proton} \approx 0.63 \cdot \sqrt{1 - 2GM / c^2 R} \cdot (B / 10^{14}\, G) \quad \text{keV}$$

Magnetars

Giant flares – a fireball model

Huge **tension** builds up in the **crust** from magnetic stress - when released this energy produces a **giant flare**.
A trapped **fireball** (orange zone) on the surface of a neutron star (brown). The fireball, containing positrons (e^+), electrons (e^-), and high-energy photons (γ), is confined by the magnetic field (dark, arched lines). It loses energy by **emitting hard X-ray photons** (orange squiggley arrows) from its surface. The fireball also contains a trace of heavy particles (protons and ions) which were blown off the surface of the neutron star. These heavy particles settle down along field lines as the fireball loses energy and shrinks.

Robert C. Duncan, University of Texas at Austin

Magnetars

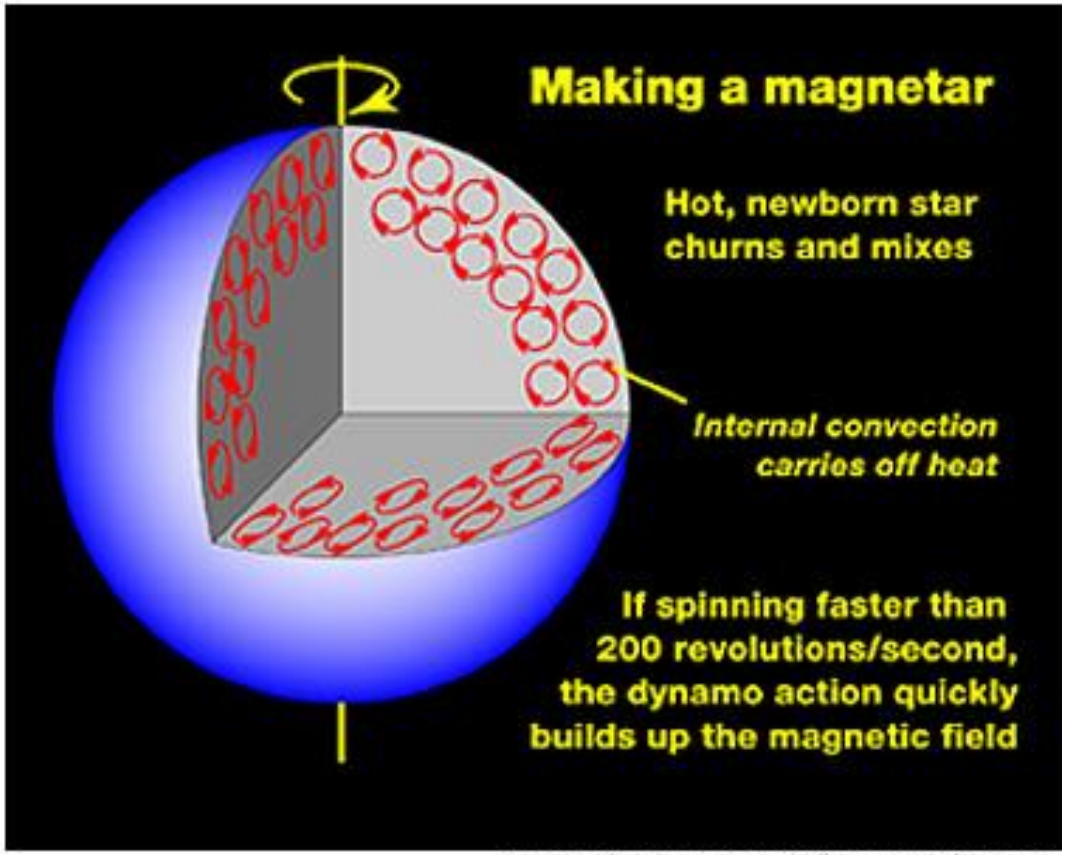

Dave Dooling, NASA Marshall Space Flight Center

Magnetars: AXPs

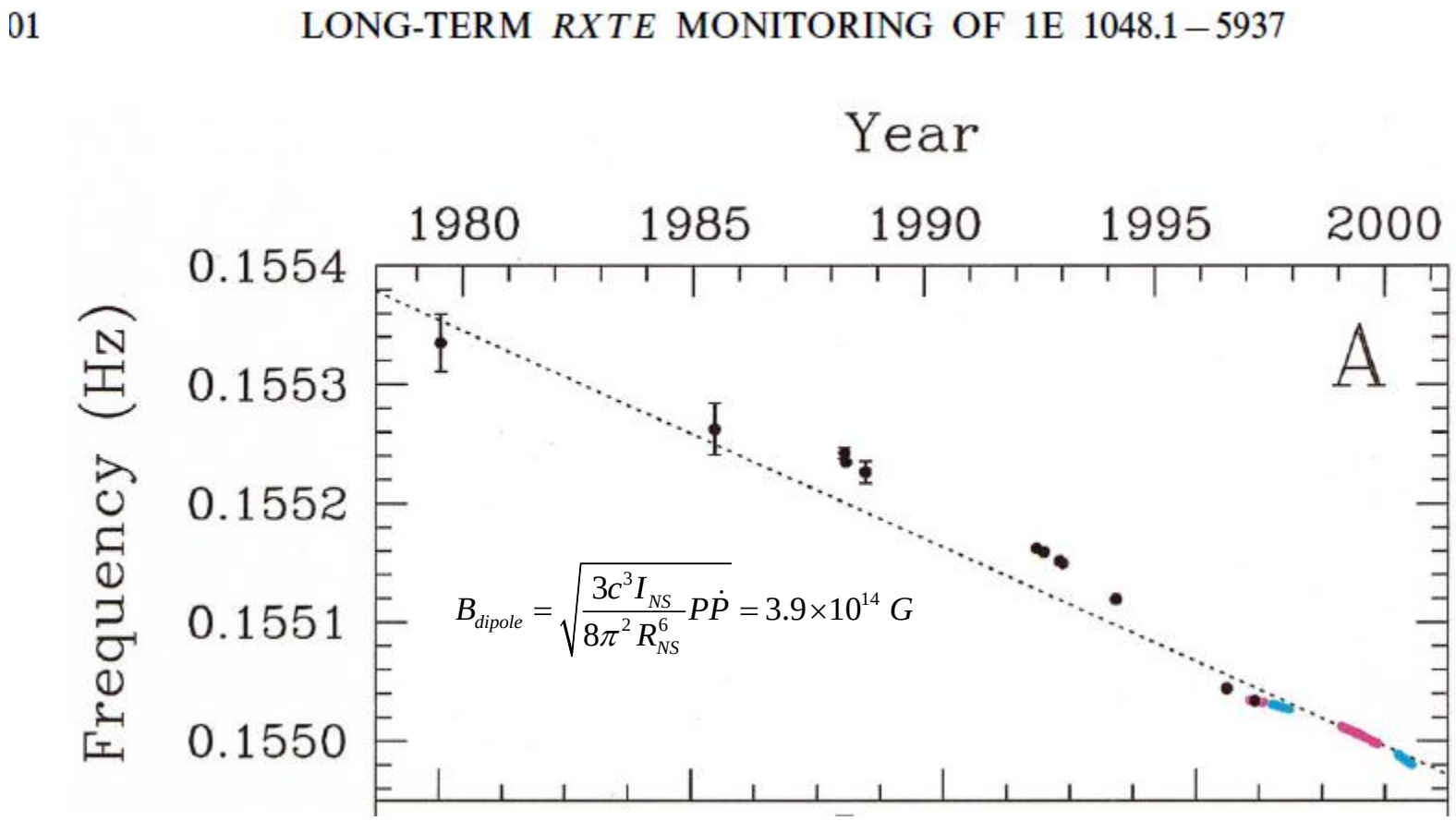

Kaspi et al. (2001), ApJ. 558, 253

Grand Unification of Neutron Stars

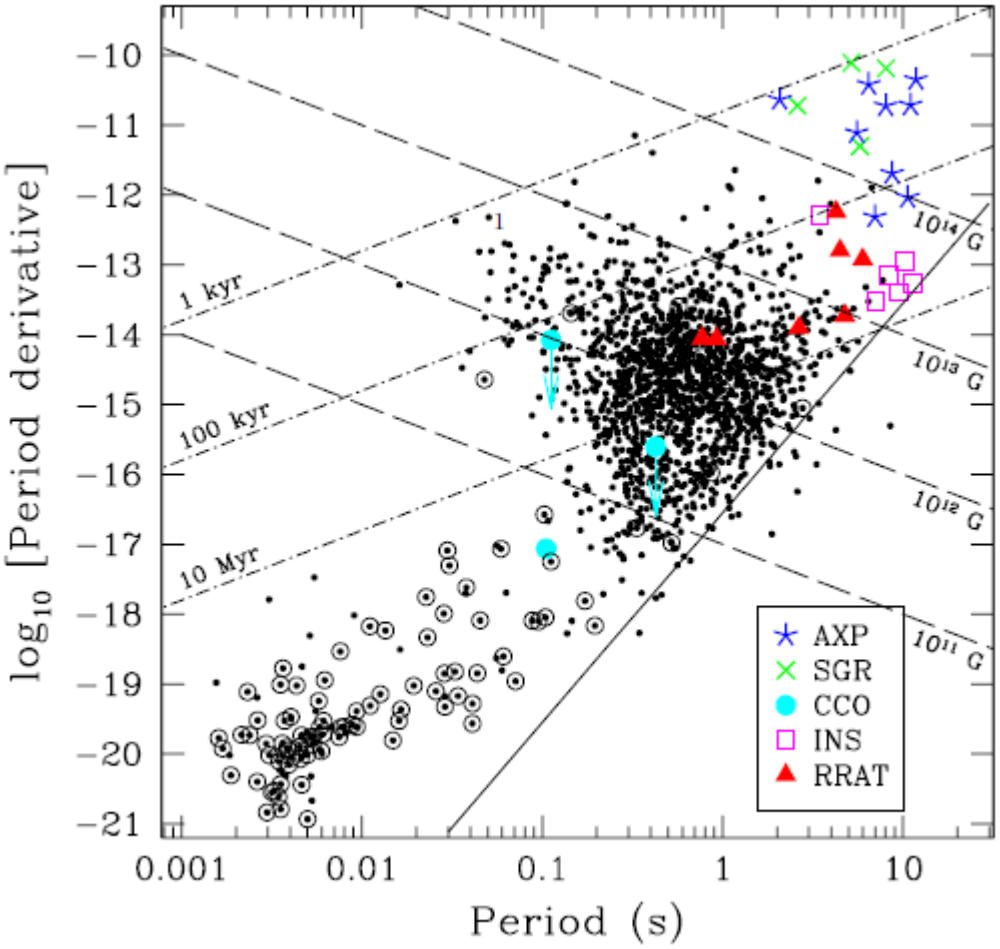

Magnetars are born with rapid spin which creates extremely high B-fields due to convection < 10 sec.

XDINs also have high B-fields.

Radio pulsars are born with moderate B-fields (**RRATs** is a subpopulation).

CCOs (”anti-magnetars”) are born with weak B-fields.

Maybe these neutron star populations are connected with their **evolution** (cf. some radio pulsars have very small brakning indices and evolve *upward* in the PP_{dot}-diagram).
Espinoza et al. (2011), ApJ, 741, L13

BH spin

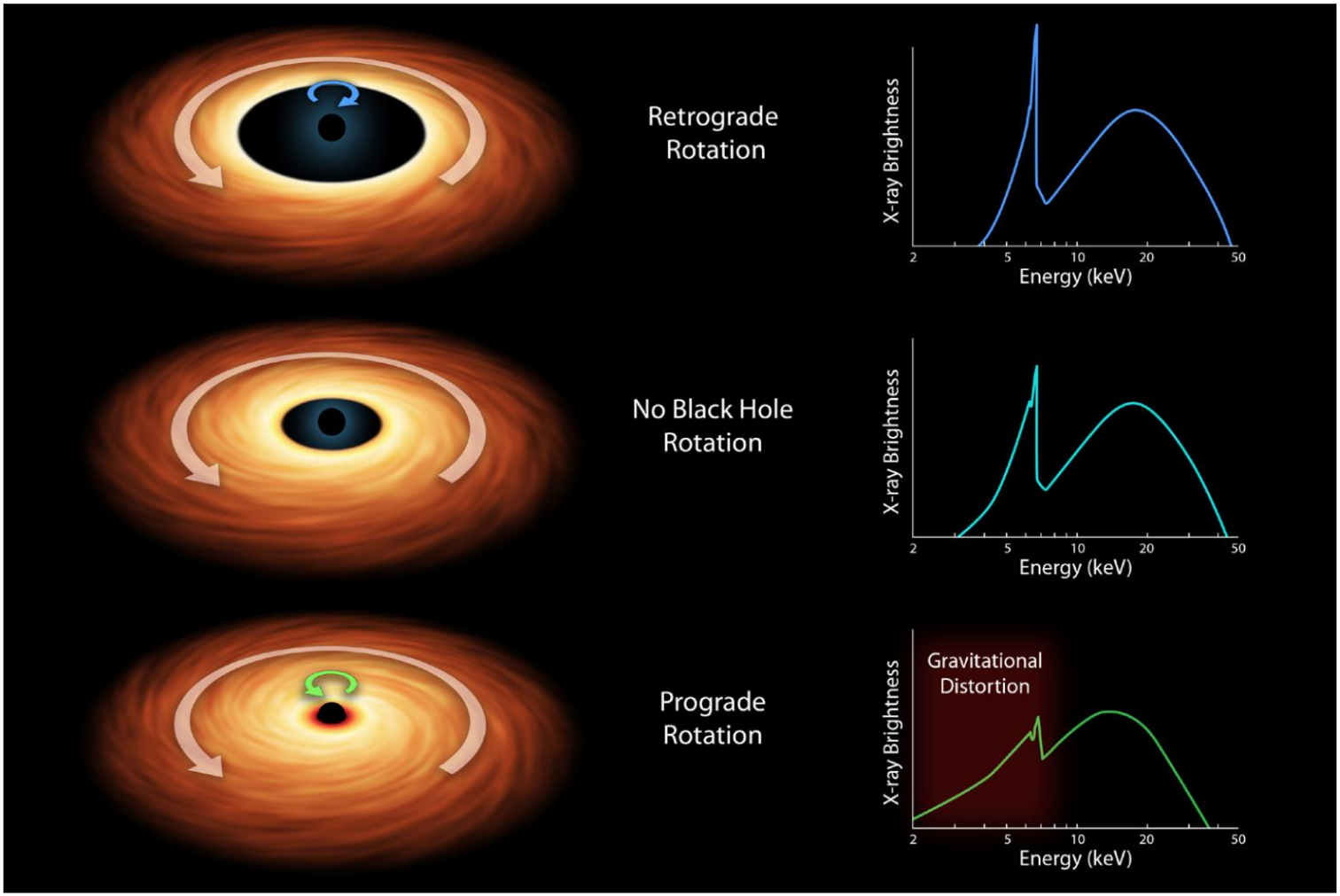

Figure 7.20: Illustration of the relation between BH spin and the location of the innermost stable circular orbit (ISCO) which can determined from the accretion disk spectrum in BH X-ray binaries. Credit: NASA/JPL-Caltech.

The BH spin can be estimated in X-ray binaries via:

1. X-ray continuum spectrum (e.g. McClintock, Narayan & Steiner 2013)
2. Relativistically broadened iron line (e.g. Reynolds 2013)
3. Quasi-periodic oscillations (e.g. Dokuchaev 2013, Motta et al. 2014)

By measuring the radius of the innermost stable circular orbit, R_{ISCO} one can obtain the spin parameter a_*

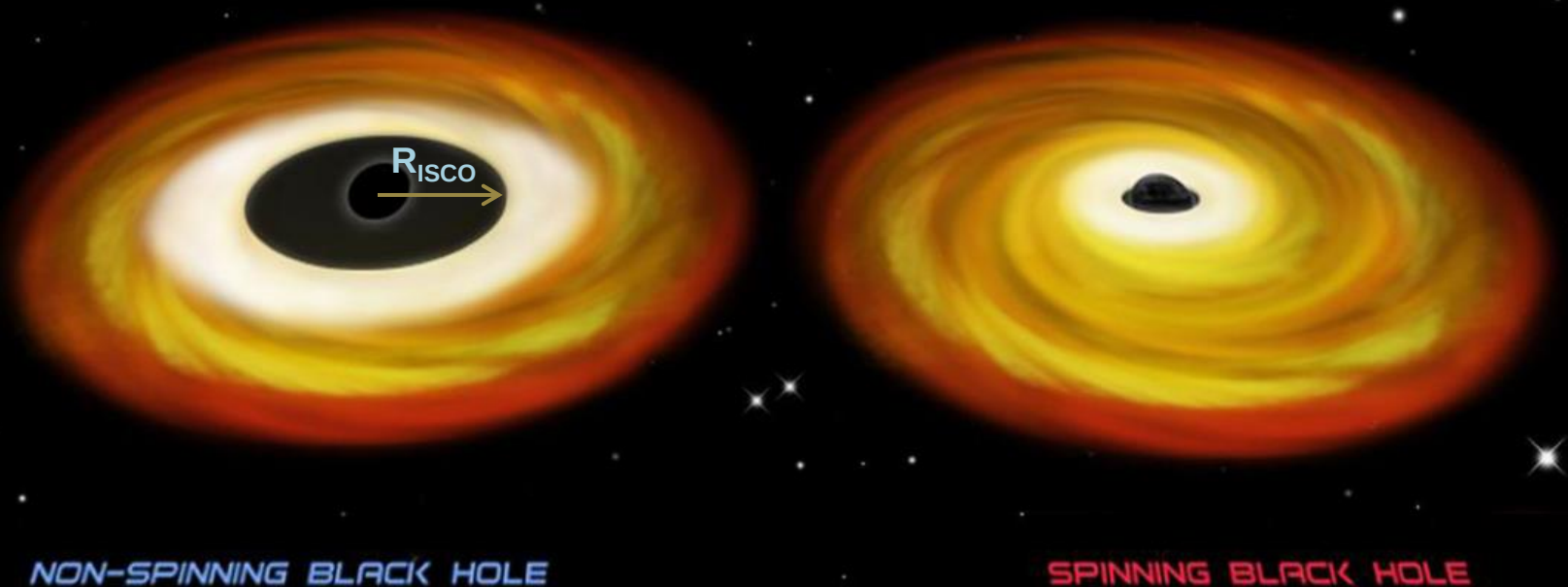

$$R_{isco} = \begin{cases} 9\ GM/c^2 & a_* = -1 \\ 6\ GM/c^2 & a_* = 0 \\ 1\ GM/c^2 & a_* = 1 \end{cases}$$

$$R_H = \begin{cases} 1\ GM/c^2 & a_* = -1 \\ 2\ GM/c^2 & a_* = 0 \\ 1\ GM/c^2 & a_* = 1 \end{cases}$$

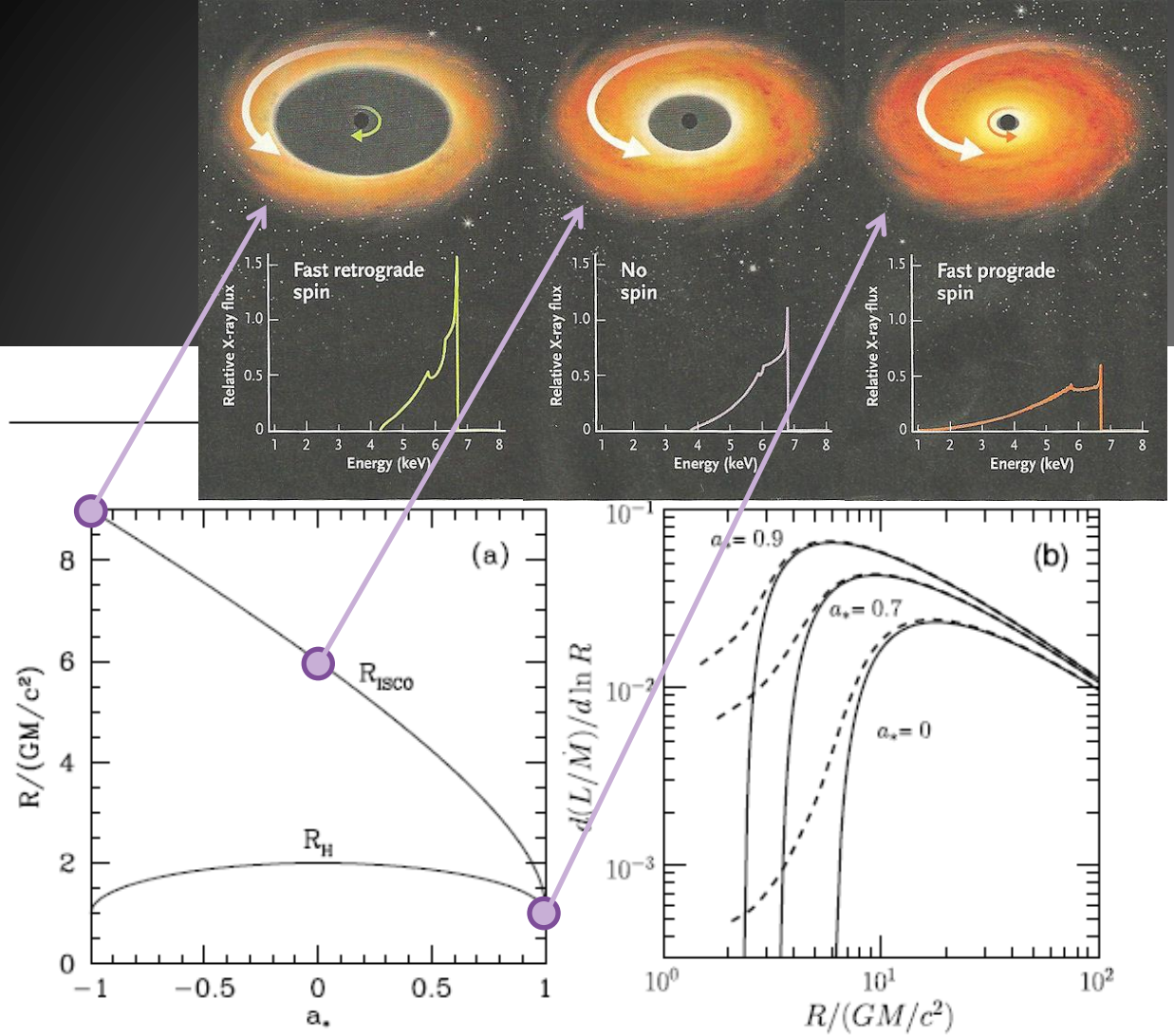

Fig. 3 (a) Radius of the ISCO $R_{\rm ISCO}$ and of the horizon $R_{\rm H}$ in units of GM/c^2 plotted as a function of the black hole spin parameter a_*. Negative values of a_* correspond to retrograde orbits. Note that $R_{\rm ISCO}$ decreases monotonically from $9GM/c^2$ for a retrograde orbit around a maximally spinning black hole, to $6GM/c^2$ for a non-spinning black hole, to GM/c^2 for a prograde orbit around a maximally spinning black hole. (b) Profiles of $d(L/\dot{M})/d\ln R$, the differential disk luminosity per logarithmic radius interval normalized by the mass accretion rate, versus radius $R/(GM/c^2)$ for three values of a_*. Solid lines are the predictions of the NT model. The dashed curves from Zhu et al. (2012), which show minor departures from the NT model, are discussed in Section 5.2.

The disk spectrum (peak emission and temperature) depends on R_{ISCO}.

Hence, R_{ISCO} and thus a_* can be determined from continuum fitting.

The solution to Einstein's equations for a rotating BH was discovered by Kerr (1963). Here shown in Boyer-Lindquist (1967) coordinates, in which the line element is given by (Shapiro & Teukolsky, Chap.12):

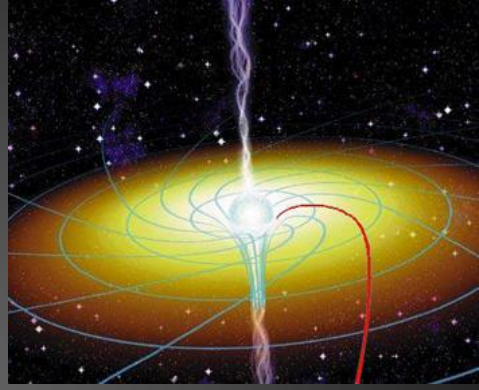

$$ds^2 = -\left(1 - \frac{2Mr}{\Sigma}\right)dt^2 - \frac{4aMr\sin^2\theta}{\Sigma}dt\,d\phi + \frac{\Sigma}{\Delta}dr^2 + \Sigma\,d\theta^2 + \left(r^2 + a^2 + \frac{2Mra^2\sin^2\theta}{\Sigma}\right)\sin^2\theta\,d\phi^2 \qquad (12.7.1)$$

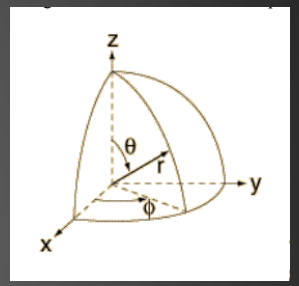

where the BH is spinning in the ϕ direction, and

$$a \equiv \frac{J}{M}, \qquad \Delta \equiv r^2 - 2Mr + a^2, \qquad \Sigma \equiv r^2 + a^2\cos^2\theta, \qquad (\text{note} \quad G = c = 1)$$

$$\wedge \quad a_* \equiv \frac{a}{M} \quad \left(a_* = \frac{Jc}{GM^2}\right)$$

Setting a=0 yields the Schwarzchild metric for a non-spinning BH. The $dt\,d\phi$ term shows the rotational frame-dragging properties of a spinning BH.

The event horizon, R_H is found when the dr^2 term in the line element becomes singular, i.e. when $\Delta=0$, or:

$$R_{H\pm} = M \pm \sqrt{M^2 - a^2}$$

$$a_* = 0 \quad \Rightarrow \quad \{R_{H+} = 2M, \quad R_{H-} = 0\}$$
$$a_* = 1 \quad \Rightarrow \quad \{R_{H+} = R_{H-} = M\}$$

Note, only R_{H+} has an astrophysical meaning.

The effective potential felt by particles orbiting a BH is given by:

$$V \equiv E^2\left(r^3 + a^2 r + 2Ma^2\right) - 4aMEl - (r - 2M)l^2 - m^2 r\Delta \qquad (12.7.15)$$

where E, l and m are the binding energy, ang. mom. and particle mass.

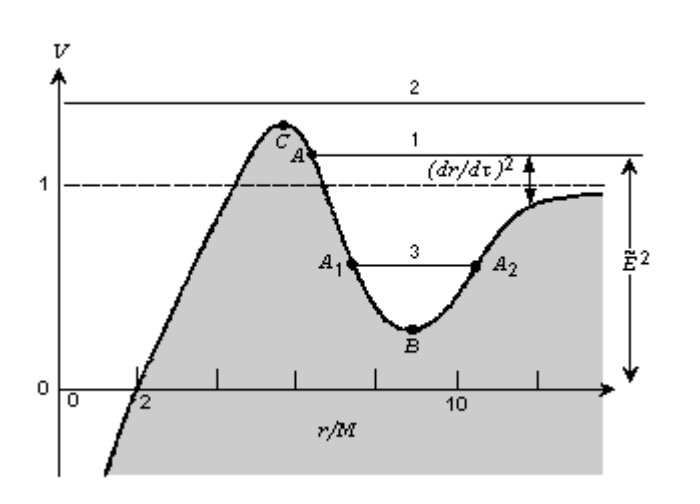

non-radial motion of test particles (S&T Fig.12.2)

2. goes straight into BH (capture)

1. bounces off and escapes BH (unbound)

3. trapped orbit around BH (bound)

B. Stable circular orbit
C. Unstable circular orbit

For circular orbits, the specific energy and the specific ang. mom. are:

$$\frac{E}{m} = \frac{r^2 - 2Mr \pm a\sqrt{Mr}}{r\sqrt{r^2 - 3Mr \pm 2a\sqrt{Mr}}} \qquad (12.7.17)$$

$$\frac{l}{m} = \frac{\sqrt{Mr}\left(r^2 \mp 2a\sqrt{Mr} + a^2\right)}{r\sqrt{r^2 - 3Mr \pm 2a}} \qquad (12.7.18)$$

The so-called photon radius is a singularity in the above equations
(solving for the denominators being equal to zero):

$$r_{ph} = 2M\left\{1 + \cos\left[\frac{2}{3}\cos^{-1}\left(\mp a/M\right)\right]\right\} \qquad (12.7.21)$$

$$a_* = \{-1, 0, 1\} \quad \Rightarrow \quad r_{ph} = \{4M, 3M, 1M\}$$

A **photon sphere** is a spherical region of space where gravity is strong enough that photons are forced to travel in orbits.

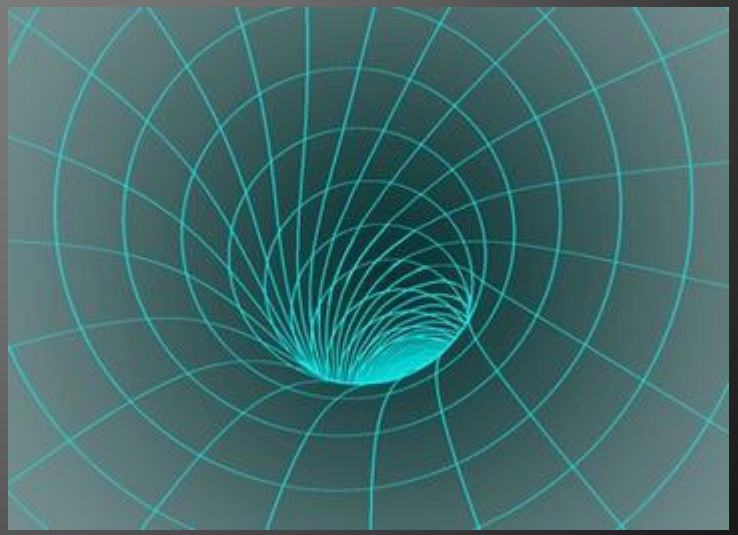

In GR, circular orbits can exist from $r = \infty$ to $r = r_{ph}$, and these can be both bound or unbound. Furthermore, not all bound orbits are *stable*. Using the stability criterion: $\partial^2 V/\partial r^2 = 0$ yields (after some algebra!):

$$R_{isco} = M\left\{3 + Z_2 \mp \left[(3 - Z_1)(3 + Z_1 + 2Z_2)\right]^{1/2}\right\} \quad (12.7.24)$$

$$Z_1 \equiv 1 + \left(1 - a^2/M^2\right)^{1/3}\left[\left(1 + a/M\right)^{1/3} + \left(1 - a/M\right)^{1/3}\right],$$

$$Z_2 \equiv \left(3a^2/M^2 + Z_1^2\right)^{1/2}$$

$$a_* = \{-1, 0, 1\} \quad \Rightarrow \quad R_{isco} = \{9M, 6M, 1M\}$$

Innermost Stable Circular Orbit (ISCO)
Bardeen (1972)

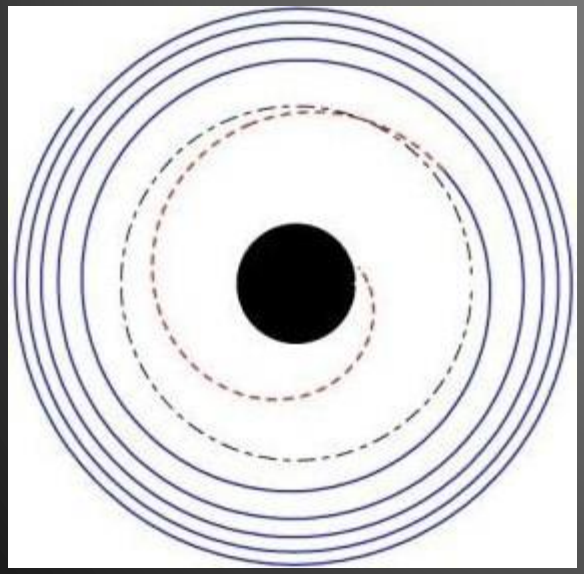

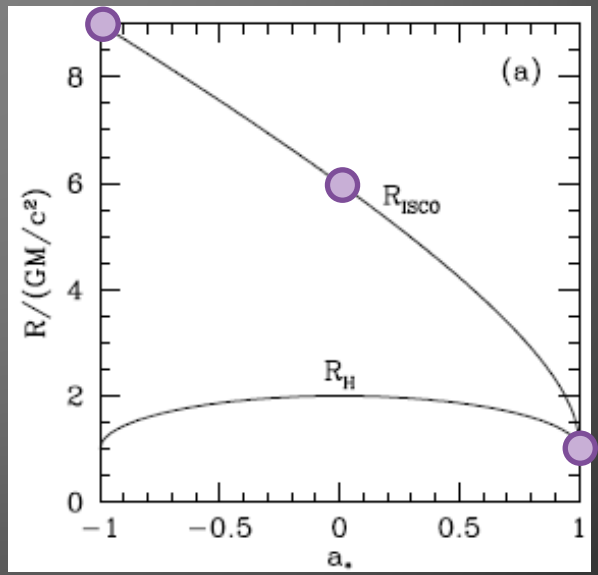

The binding energy* at the ISCO is important for the accretion luminosity:

$$a_* = \frac{a}{m} = \underset{\text{plus}}{\mp} \frac{4\sqrt{2}\sqrt{1-(E/m)^2} - 2E/m}{3\sqrt{3}\left(1-(E/m)^2\right)} \qquad (12.7.25)$$

$$a_* = \{-1, 0, 1\} \quad \Rightarrow \quad E/m = \left\{\sqrt{25/27}, \sqrt{8/9}, \sqrt{1/3}\right\}$$

Realistic accretion disks with B-fields may change this slightly…

Thus the maximum energy release is: $1-\sqrt{1/3} \approx 0.423$ of rest-mass energy!

(For a non-spinning BH the energy release is: $1-\sqrt{8/9} \approx 0.057$)

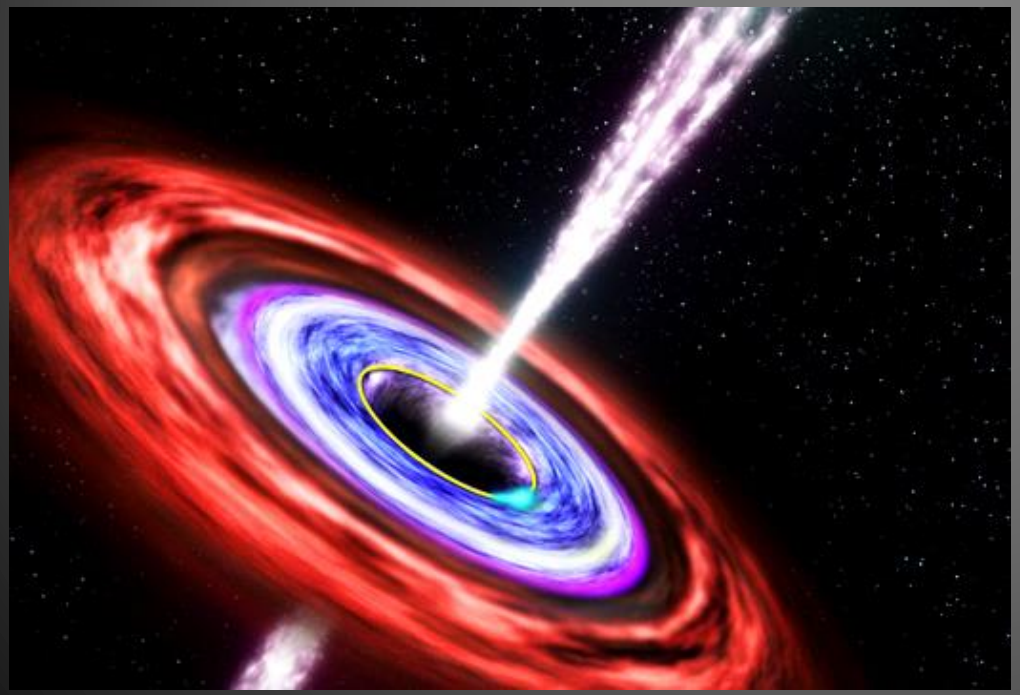

* Defined to be zero at event horizon? (and not at infinity? Hence, 1-E?)

Table 7.3: Measured values of BH spins (a_*) using the continuum-fitting method. (After McClintock et al., 2014; Zhao et al., 2020; Reynolds, 2020; Miller-Jones et al., 2021, and references therein).

Tauris & van den Heuvel (2022)

Source	BH spin (a_*)	BH mass ($M_{\rm BH}/M_\odot$)
Persistent X-ray binaries		
Cyg X-1	> 0.9985*	21.2 ± 2.2
LMC X-1	$0.92^{+0.05}_{-0.07}$	10.9 ± 1.4
IC 10 X-1	$0.85^{+0.04}_{-0.07}$	15 (assumed)
M33 X-7	0.84 ± 0.05	15.65 ± 1.45
Transient X-ray binaries		
GRS 1915+105	> 0.95	10.1 ± 0.6
4U 1543−47	0.80 ± 0.10	9.4 ± 1.0
GRO J1655−40	0.70 ± 0.10	6.3 ± 0.5
Nova Mus 1991	$0.63^{+0.16}_{-0.19}$	11.0 ± 1.8
XTE J1550−564	$0.34^{+0.20}_{-0.28}$	9.1 ± 0.6
LMC X-3	< 0.3	7.6 ± 1.6
H1743−322	0.2 ± 0.3	~ 8
MAXI J1820+070	$0.13^{+0.07}_{-0.10}$	8.5 ± 0.7
A0620−00	0.12 ± 0.19	6.6 ± 0.25

* Assuming aligned spin. ($\delta = 15^\circ$ yields $a_* = 0.9696$, Miller-Jones et al., 2021).

The spins of the persistent BHs must be natal:

The accretion rate onto a BH is Eddington limited and the time interval of accretion is also limited by the age of the companion star.

Consider **Cyg X-1**:
To acheive $a_* > 0.95$ requires accretion of $> 7.3\, M_\odot$ if the BH was born non-spinning (Bardeen 1970; King & Kolb 1999).
For Eddington-limited accretion this requires: $\tau_{spin-up} \approx 31\, Myr$.
However, the age of the system is only $\tau_{nuc} \approx 4-7\, Myr$ (Wong et al. 2012).

Also for **M33 X-7** and **LMC X-1** is $\tau_{spin-up} \gg \tau_{nuc}$ (factor 5-6)
McClintock, Narayan & Steiner (2013).

Hence, these BH are *born rapidly spinning*.

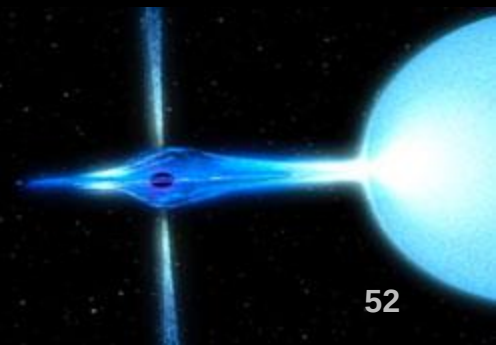

BHs may lose spin in jets (or from the Penrose process)

Poloidal B-field are twisted by frame-dragging, thereby producing outgoing Poynting flux along twin jets. Ruffini & Wilson (1975); Blandford & Znajek (1977)

Modern GRMHD simulations show that the power carried by the jet exceeded the total rest mass energy of accreted mass. Tchekhovskoy et al. (2011)

$$\eta_{jet} \equiv \left\langle L_{jet} \right\rangle / \dot{M}c^2$$

McClintock, Narayan & Steiner (2013)

$$\eta_{jet} \propto \Omega_H^2$$

$$\Omega_H = \frac{c^3}{2GM}\left(\frac{a_*}{1+\sqrt{1-a_*^2}}\right)$$

Angular velocity at the BH horizon

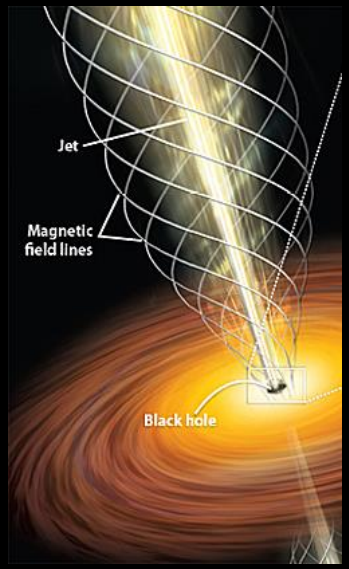

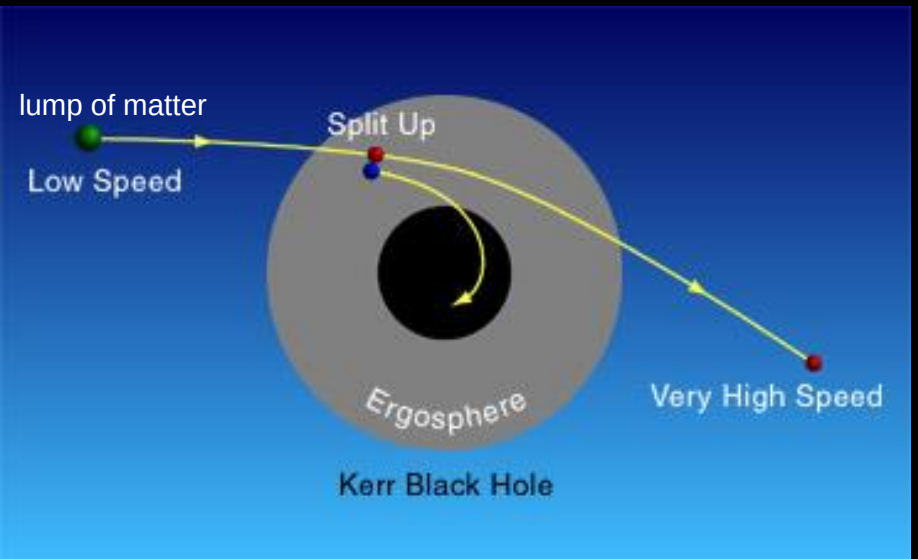

Inside the ergosphere spacetime is dragged along, causing matter being forced to corotate. In principle, rotational energy of the BH can be extracted from the ergosphere by the Penrose (1969) process.

Summary

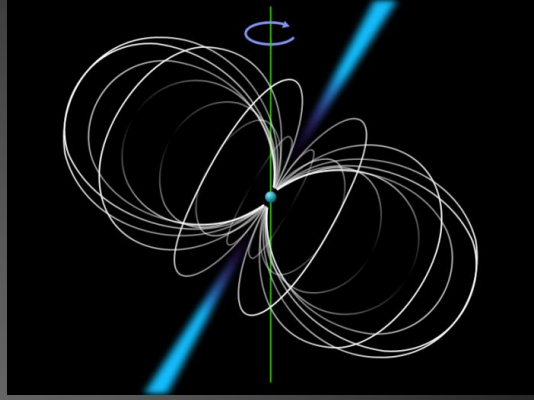

- Observational aspects of radio pulsars
  - The radio pulsar population in the Milky Way
  - Pulse profiles / Scintillation / Dispersion measure
  - Emission properties
- Spin evolution of pulsars in the *PP*-diagram
  - The magnetic dipole model
  - Gravitational wave emission
  - Evolution with B-field decay
  - Evolution with gravitational wave emission
  - The braking index
  - True ages of radio pulsars
- Magnetars
  - Soft gamma-ray repeaters (SGRs) and Anomalous X-ray pulsars (AXPs)
- BH spins
  - BHs in X-ray binaries (continuum spectrum fitting)
  - Origin and evolution of X- binary BH spins

Self-study of equations

Albert-Einstein Institute Lectures 2021

Thomas Tauris @ Aarhus University

Lectures 1+2: Wednesday May 12, 10:00 – 12:00

X-ray Binaries and Recycling Millisecond Pulsars

Lectures 3+4: Friday May 14, 10:00 – 12:00

Spin and B-field Evolution of Neutron Stars (+ Black Hole Spins)

Lectures 5+6: Wednesday May 19, 10:00 – 12:00

Formation of Binary Neutron Stars/Black Holes

Lectures 7+8: Friday May 21, 10:00 – 12:00

Binary Neutron Stars and Gravitational Waves at Low and High Frequencies

You are most welcome to ask questions any time ☺